Available online at www.sciencedirect.com
SCIENCE DIRECT
Journal of Sound and Vibration 294 (2006) 752–779
JOURNAL OF SOUND AND VIBRATION
www.elsevier.com/locate/jsvi

Spectral and multiresolution Wiener expansions of oscillatory stochastic processes

C.L. Pettit[a,*], P.S. Beran[b]

[a]Aerospace Engineering Department, United States Naval Academy, Annapolis, MD 21402, USA
[b]Air Vehicles Directorate, United States Air Force Research Laboratory, Wright-Patterson AFB, OH 45433, USA

Received 1 April 2005; received in revised form 17 November 2005; accepted 4 December 2005
Available online 9 March 2006

Abstract

Wiener chaos expansions are being evaluated for the representation of stochastic variability in the response of nonlinear aeroelastic systems, which often exhibit limit cycles. Preliminary studies with a simple nonlinear aeroelastic computational model have shown that the standard non-intrusive Wiener–Hermite expansion fails to maintain time accuracy as the simulation evolves. Wiener–Hermite expansions faithfully reproduce the short-term characteristics of the process but consistently lose energy after several mean periods of oscillation. This energy loss remains even for very high-order expansions. To uncover the cause of this energy loss and to explore potential remedies, the more elementary problem of a sinusoid with random frequency is used herein to simulate the periodic response of an uncertain system. As time progresses, coefficients of the higher order terms in both the Wiener–Hermite and Wiener–Legendre expansions successively gain and lose dominance over the lower-order coefficients in a manner that causes any fixed-order expansion in terms of global basis functions to fail over a simulation time of sufficient duration. This characteristic behavior is attributed to the continually increasing frequency of the process in the random dimension. The recently developed Wiener–Haar expansion is found to almost entirely eliminate the loss of energy at large times, both for the sinusoidal process and for the response of a two degree-of-freedom nonlinear system, which is examined as a prelude to the stochastic simulation of aeroelastic limit cycles. It is also found that Mallat's pyramid algorithm is more efficient and accurate for evaluating Wiener–Haar expansion coefficients than Monte Carlo simulation or numerical quadrature.

1. Introduction

The need to revolutionize methods of assessing aeroelastic stability has become increasingly pressing in recent years. This is driven primarily by two factors: (1) the desire to greatly reduce the total cost of certification by reducing testing requirements, and (2) the emergence of unique design concepts intended to provide impressive performance gains, especially in military applications. A common feature of these designs is that they substantially increase the potential for nonlinear behavior beyond levels that can be adequately addressed by current engineering tools and processes.

*Corresponding author. Tel.: +1 410 293 6415; fax: +1 410 293 2591.
E-mail addresses: pettitcl@usna.edu (C.L. Pettit), philip.beran@wpafb.af.mil (P.S. Beran).

0022-460X/$ - see front matter © 2006 Elsevier Ltd. All rights reserved.
doi:10.1016/j.jsv.2005.12.043

Nomenclature

$\mathrm{He}_j(\xi)$	jth polynomial chaos of ξ
$L^2(\mathbb{R})$	set of square-integrable real-valued functions on $\mathbb{R}$
$m(y) = \mathrm{d}M/\mathrm{d}y$	probability density function
$M(y) = \mu((-\infty, y])$	probability distribution function
N	number of time samples
n	number of process realizations
P	order of polynomial chaos expansion
$P^{(j)}$	projection on jth scale of Haar basis
$\Pr(\theta)$	probability of event θ
$\mathbb{R}$	set of real numbers
t	time
$x(t, \xi)$	random process
$\hat{x}_j(t)$	polynomial chaos coefficient
y	an allowable value of a random variable
$\mathbb{Z}$	set of integers
z	uniform random variable
θ	random variable
$\mu((-\infty, y])$	probability distribution
ξ	random variable
σ_ω	standard deviation of frequency
ω	angular frequency
ω_0	mean angular frequency
$\langle\cdot\rangle$	expected value operator

These issues were the focus of a recent workshop organized by the Air Force Office of Scientific Research (AFOSR) and the Air Force Research Laboratory (AFRL) [1]. The workshop addressed traditional areas of concern, such as the basic physics and computational requirements of nonlinear aeroelasticity, but it also included sessions on model verification and validation (V&V) as well as the role of uncertainty quantification (UQ) in understanding the physics of nonlinear aeroelasticity and certifying aeroelastic stability. The participants of the workshop developed a strong consensus that UQ must play a prominent role in future aeroelasticity research; in particular, it was agreed that UQ could provide a common language for promoting communication between analysts and test personnel.

Probabilistic methods for linear systems have been employed in gust analysis [2] for several decades, but probabilistic study of aeroelastic stability is a relatively recent development. Current research trends differ conceptually from standard gust analysis, which assumes variability only in the gust velocity and depends on linear structural dynamics to develop equivalent static design loads; thus, gust analysis forces an inherently probabilistic process to conform to our deterministic engineering philosophy. In contrast, recent research is the outgrowth of a more holistic perspective on the role of uncertain system and environment properties in establishing the probability of aeroelastic stability. This approach can produce insight in all aeroelastic stability studies, but the payoff likely will be greatest in analyzing the time-dependent behavior of nonlinear systems owing to their generally higher sensitivity [3–6].

Liaw and Yang [7,8] examined aeroelasticity of laminated plates and shells with uncertainties in several structural and geometric parameters. Their work appears to represent the first published application of a stochastic finite element method (SFEM) to the analysis of aeroelastic stability. Their approach involved a second-moment, perturbation-based stochastic finite element model. They described the effects of variability on the likely range of responses, but because they employed a second-moment formulation, quantification of output variability was limited to estimates of the amplitude standard deviation.

Lindsley et al. [9–11] also studied limit-cycle oscillations (LCO) of panels with spatial variability in the modulus of elasticity and the thermal expansion coefficient, but they employed Monte Carlo simulation (MCS) to better quantify the distribution of response variability in this nonlinear system. They limited their analysis to square panels and isotropic materials, but also included the influence of non-ideal boundary conditions (BCs) so as to measure the relative importance of uncertainty in material properties and BCs. These studies showed that relatively minor levels of variability in system parameters, loads, and BCs can induce significant changes in the stability of nonlinear aeroelastic systems.

Given the high computational cost associated with time-accurate simulation of practical stochastic systems, stochastic expansions are being pursued both to accelerate the analysis and to provide a mathematical basis for assessing the convergence of the response statistics [12,13]. Aeroelastic limit cycles, which commonly are referred to as LCO, are known to be sensitive to parametric uncertainty [3], so our goal is to investigate the suitability of stochastic expansions to modeling the occurrence and variability of LCO.

As a first step in this direction, we have formulated a model problem that exhibits the essential temporal characteristics of limit cycles. This simple problem involves a sinusoidal process for which the frequency of each realization is a random variable. It is found that the common spectral stochastic expansion, such as the Wiener–Hermite (WHe) and Wiener–Legendre (WLe) expansions, perform poorly in the time domain modeling of periodic processes; specifically, non-intrusive WHe and WLe expansions faithfully reproduce the short-term characteristics of the sinusoidal process but consistently lose energy after several mean periods of oscillation. This energy loss remains even for very high-order expansions, which suggests that spectral stochastic expansions should not be employed to model limit cycles. This does not appear to have been discussed thoroughly in the literature, so we carefully explore the sinusoidal model problem with the goal of motivating alternative methods for simulating systems that exhibit LCO.

Millman et al. [14] have also noted the failure of spectral stochastic expansions for representing limit cycles. The present paper is somewhat complementary in that Millman et al. did not analyze the convergence difficulties in detail; instead, they proposed a modified Wiener expansion that employed Fourier basis functions on a truncated random domain. Also, they employed a Galerkin projection of the governing equations onto the Fourier-based chaoses instead of the MCS approach employed herein. Their Fourier-based approach partially resolved the large-time inadequacy of the WHe expansion, but the probabilistic convergence was inadequate, especially in the tails of the response distribution.

An alternative means of overcoming the loss of energy in Wiener-based simulation of limit cycles is demonstrated herein. Haar basis functions [15,16] are used instead of global (e.g., Hermite or Legendre) basis functions in the random dimension to provide a localized representation of the stochastic process's temporal evolution. It is demonstrated below that the efficacy of this wavelet-based expansion follows from its ability to localize the continually increasing nonlinearity of the process in the random dimension. Two approaches for evaluating the Wiener–Haar (WHa) expansion coefficients are presented and compared. One is based on MCS; the other uses Mallat's pyramid algorithm, which is commonly referred to as the discrete wavelet transform.

2. Chaos expansions of stochastic processes

The theory of global and local Wiener chaos expansion is presented along the line established recently by Le Maître et al. [16]. The discussion begins with a brief description of the probability nomenclature employed throughout the subsequent discussion. This is followed in turn by summaries of single variable polynomial chaos expansions (PCE), wavelet or multiresolution analysis and synthesis of deterministic functions, and the marriage of Wiener expansions with multiresolution analysis.

2.1. Probability background

We assume θ is an outcome in a probability space, $\xi(\theta)$ is a random variable (rv) that maps outcomes from the probability space to $\mathbb{R}$, and $y \in \mathbb{R}$ is a possible value of ξ. This rv follows a specified distribution function,

$$M_\xi(y) = \mu_\xi((-\infty, y]) = \Pr[\theta : \xi(\theta) \leqslant y],$$

where the induced measure, μ, is the associated distribution of ξ. We assume that $M_\xi(y)$ is continuous and strictly increasing. Under these conditions, $\mathrm{d}M_\xi(y) = m_\xi(y)\,\mathrm{d}y$ defines the probability density induced by $\xi(\theta)$ and there exists for any $z \in [0, 1]$ a unique $\{y : M_\xi(y) = z\}$; furthermore, this mapping can be inverted to obtain $y = M_\xi^{-1}(z)$. In the applications considered here, the rv $\xi(\theta)$ is assumed to be a random system property and $x(t, \xi(\theta))$, a stochastic process, is the associated response. With these definitions, an individual realization of the process is $x(t, y)$.

The expected value operator of the process for any time t is written as

$$Ex(t) = \langle x(t, \xi)\rangle = \int x(t, \xi(\theta))\,\Pr(\mathrm{d}\theta) = \int_{-\infty}^{\infty} x(t, y)\mathrm{d}M_\xi(y). \tag{1}$$

2.2. Global bases for the random dimension

Only the primary ingredients of PCE are summarized here. Ghanem and Spanos [12] present a comprehensive development of the theory, and Xiu and Karniadakis [13,17], Le Maître et al. [18], and Walters [19] describe some relevant recent applications.

The PCE provides an orthogonal expansion of a random process whose covariance operator is unknown, such as the response of a nonlinear system to a normal or non-normal input. Instead of expanding the process in terms of normal rvs, as in the Karhunen–Loeve expansion [12,20], the underlying random variables are replaced by orthogonal polynomials of random variables, which often are assumed to be normal or uniform. When the variables are normal, this expansion is also known as the Hermite chaos or WHe expansion because the Hermite polynomials are orthogonal with respect to the Gaussian measure. If the rv are uniformly distributed on some finite interval or rectangle, a similar expansion can be employed with the Legendre polynomials as the basis; this will be referred to as the WLa expansion. The WLe development is omitted because it directly parallels that which is presented here for WHe. Generalized PCE for other probability distributions and their associated bases have been described recently by Xiu and Karniadakis [13].

Our presentation assumes that the process of interest, $x(t,\xi)$, is governed by a single Gaussian random variable, ξ, which can always be normalized to have zero mean value and unit standard deviation. The stochastic process is approximated by a truncated series,

$$x(t,\xi(\theta)) = \sum_{j=0}^{P} \hat{x}_j(t)\mathrm{He}_j(\xi(\theta)), \tag{2}$$

where $\{\hat{x}_j(t)\}$ are generalized Fourier coefficients and $\{\mathrm{He}_j(\xi)\}$ are the Hermite polynomials in ξ, which are orthogonal with respect to the Gaussian measure, $\mathrm{d}M_\xi(y) = \mathrm{e}^{-y^2/2}\,\mathrm{d}y$; these polynomials are referred to as the polynomial chaoses. The expansion in Eq. (2) is guaranteed to converge as $P \to \infty$ for any square-integrable process, where square-integrability must be with respect to the Gaussian probability measure. Expansions for multiple rv can be developed by extending the single-variable relations into product spaces of independent normal random variables [12].

The Hermite polynomials can be generated from the following recurrence relation:

$$\mathrm{He}_0 = 1, \quad \mathrm{He}_1 = \xi, \quad \mathrm{He}_j = \xi\mathrm{He}_{j-1} - (j-1)\mathrm{He}_{j-2}. \tag{3}$$

In terms of the expected value operator defined in Eq. (1), these satisfy $\langle \mathrm{He}_i\mathrm{He}_j\rangle = 0$ for $i \neq j$; that is, the polynomial chaoses are statistically orthogonal and the generalized Fourier coefficients can be evaluated directly:

$$\hat{x}_j(t) = \frac{\langle x\mathrm{He}_j\rangle}{\langle \mathrm{He}_j^2\rangle}. \tag{4}$$

The denominator in Eq. (4) can be shown to satisfy $\langle \mathrm{He}_j^2\rangle = j!$, so the key step in projecting $x(t,\xi)$ on the polynomial chaoses is the evaluation of $\langle x\mathrm{He}_j\rangle$. Eqs. (2)–(4) can be combined to show that $\hat{x}_0(t)$ represents the time-dependent expected value of the process and $\sum_{j=1}^{P}(\hat{x}_j(t))^2$ approaches the time-dependent variance as $P \to \infty$.

Standard MCS was employed in this study to estimate the expected value in Eq. (4). More efficient approaches that could be considered for practical implementation include the many variance reduction or efficient sampling techniques [21,22], which should improve the convergence of the MCS, and Gauss–Hermite quadrature of the integral in Eq. (1). However, the results presented below show that oscillatory random processes become increasingly oscillatory in the random dimension as time progresses; moreover, bifurcations can make these functions discontinuous. These observations suggest that even Gauss quadrature would require many samples to yield acceptable accuracy. We do not address this question further herein. Given the computational expense associated with realistic aeroelastic simulations, some combination of efficient sampling and reduced-order physics models will likely be required for more complex problems. Pettit [6] discusses this concern in slightly greater depth.

2.3. Local bases for the random dimension

Results provided below show that the global PCE bases are inadequate for representing stochasticity of limit cycles. A wavelet-based generalization of the PCE is described here in preparation for its use to address this inadequacy. The discussion is limited to the Haar basis, which constitutes the most elementary multiresolution analysis (MRA) of $L^2(\mathbb{R})$ [15,23].

2.3.1. Haar wavelet series

The Haar scaling function is defined by

$$\phi(t) = \mathbf{I}_{[0,1)}(t) = \begin{cases} 1, & 0 \leqslant t < 1, \\ 0 & \text{otherwise}, \end{cases} \tag{5}$$

where $\mathbf{I}_{[a,b)}(t)$ is the indicator function for $t \in [a, b)$. Scaled and translated version of $\phi(t)$ are written as

$$\phi_k^{(j)} = 2^{j/2}\phi(2^j t - k), \tag{6}$$

where $j \in \{\mathbb{Z} \geqslant 0\}$, $k \in [0, 2^j - 1]$, and the scale factor, $2^{j/2}$ is chosen so that $\|\phi_k^{(j)}\| = 1$.

Let $x(t)$ be a square-integrable function on the unit interval. Each scale or dilation factor j defines a space, $V_j = \text{span}\{\phi_k^{(j)}\}$, of piecewise constant functions such that $V_{j-1} \subset V_j$. The set $\{\phi_k^{(j)}\}$ forms a partition of $[0, 1)$. Let $P^{(j)}x$ be the projection of x onto V_j; then

$$P^{(j)}x = \sum_{k=0}^{2^j-1} c_k^{(j)}\phi_k^{(j)}(t) \tag{7}$$

and the projection coefficients are given by the inner product

$$c_k^{(j)} = \int_0^1 x(t)\phi_k^{(j)}(t)\,\mathrm{d}t. \tag{8}$$

Increasing j therefore produces a higher resolution projection, so that the sequence of spaces $\{V_j\}_{j=0}^{\infty}$ comprise a MRA of $L^2([0, 1))$. Scaling the unit interval extends this to a MRA of $L^2(\mathbb{R})$.

Because $V_{j-1} \subset V_j$, the projection $P^{(j-1)}x$ leaves behind a detail function $w^{(j-1)} \in V_j$, which is the difference between two resolution levels:

$$w^{(j-1)} = P^{(j)}x - P^{(j-1)}x. \tag{9}$$

This difference can be represented in terms of the Haar wavelets, which are based on the piecewise-constant mother wavelet:

$$\psi(t) = \begin{cases} 1, & 0 \leqslant t < 1/2, \\ -1, & 1/2 \leqslant t < 1, \\ 0 & \text{otherwise}. \end{cases} \tag{10}$$

An orthonormal basis for $L^2(\mathbb{R})$ is composed of all possible integer-valued translations and dilations of $\psi(t)$,

$$\psi_k^{(j)}(t) = 2^{j/2}\psi(2^j t - k), \quad j, k \in \mathbb{Z}, \tag{11}$$

which satisfy $\|\psi_k^{(j)}(t)\| = 1$; therefore, any square-integrable function can be expanded in a Haar wavelet series,

$$x(t) = \sum_{j,k} d_k^{(j)}\psi_k^{(j)}(t) \tag{12}$$

and the generalized Fourier coefficients can be evaluated as

$$d_k^{(j)} = \int_{-\infty}^{\infty} x(t)\psi_k^{(j)}(t)\,\mathrm{d}t. \tag{13}$$

As for the scaling function, limiting the translation index to $k \in \{0, \ldots, 2^j - 1\}$ restricts the domain to the unit interval, $t \in [0, 1)$; therefore, the detail function can be synthesized from the wavelets at scale $j - 1$,

$$w^{(j-1)} = \sum_{k=0}^{2^j-1} d_k^{(j-1)} \psi_k^{(j-1)}(t) \tag{14}$$

and the projection $P^{(j)}x$ can be expanded as

$$P^{(j)}x = P^{(j-1)}x + \sum_{k=0}^{2^{(j-1)}-1} d_k^{(j-1)} \psi_k^{(j-1)}(t) = P^{(0)}x + \sum_{m=0}^{j-1} \sum_{k=0}^{2^m-1} d_k^{(m)} \psi_k^m(t), \tag{15}$$

$$= c_0 \phi(t) + \sum_{m=0}^{j-1} \sum_{k=0}^{2^m-1} d_k^{(m)} \psi_k^m(t). \tag{16}$$

As noted above, this decomposition can be extended directly to functions with compact support on any interval (i.e., $t \in [a, b)$ where $-\infty < a < b < \infty$). In practice, the upper resolution limit, $J = \max(j)$, must be determined by the resolution needed to retain the scales that contain significant energy. If t is restricted to a discrete set by a sampling process, the sampling interval naturally establishes an upper bound on J.

2.3.2. Wiener–Haar expansion

The localized behavior of a stochastic process in the random dimension can be represented by generalizing the Haar wavelet series described above. This approach represents a marriage of the wavelet series, which is more commonly applied to functions of time or space, with the Wiener chaos expansion. The stochastic process, $x(t, \xi)$, is written as a WHa expansion in which the wavelet coefficients, $d_k^{(j)}(t)$, are functions of time or space and the wavelet series decomposes the random dimension of the process. As noted earlier, our development follows Le Maître et al. [16].

The random variable $\xi(\theta)$ is assumed to be restricted to a finite interval $[a, b] \subset \mathbb{R}$. The extension of the Haar wavelets, $\psi_k^{(j)}$, from the unit interval to $\xi \in [a, b]$ is defined by

$$\Psi_k^{(j)}(\xi) = \psi_k^{(j)}[\Pr(\xi(\theta))], \tag{17}$$

so that individual realizations satisfy

$$\Psi_k^{(j)}(y) = \psi_k^{(j)}(z), \tag{18}$$

where y is a realization of ξ and z is a realization of a uniform rv on $[0, 1]$. This works for any $M(y)$ that is continuous and strictly increasing on $[a, b]$, so that $z = M(y)$ is one-to-one and invertible. With this definition, the orthonormality of the Haar wavelets leads to

$$\int_0^1 \psi_k^{(j)}(z) \psi_n^{(l)}(z)\, \mathrm{d}z = \int_a^b \Psi_k^{(j)}(y) \Psi_n^{(l)}(y)\, \mathrm{d}M(y) = \delta_{j,l}\delta_{k,n}, \tag{19}$$

i.e., the wavelets $\{\Psi_k^{(j)}(\xi)\}$ are orthonormal with respect to the distribution of ξ and form a MRA of the space of second-order random processes on $[a, b]$ with continuous distributions. The associated inner product is

$$\langle uv \rangle = \int_a^b u(y)v(y)m(y)\, \mathrm{d}y, \tag{20}$$

where $m(y)$ is the associated density.

With these preliminary considerations in place, the WHa expansion is written as

$$x(t, \xi(\theta)) = x_0(t) + \sum_{j=0}^{\infty} \sum_{k=0}^{2^j-1} d_k^{(j)} \Psi_k^{(j)}(\xi(\theta)), \tag{21}$$

$$= x_0(t) + \sum_{j=0}^{\infty} \sum_{k=0}^{2^j-1} d_k^{(j)} \psi_k^{(j)}(\Pr(\xi)), \tag{22}$$

where the scaling function coefficient

$$x_0(t) = P^{(0)}x, \tag{23}$$

$$= \int_0^1 x(t, M^{-1}(z))\phi_0(z)\,\mathrm{d}z, \tag{24}$$

$$= \int_a^b x(t, y)\,\mathrm{d}M(y) = \langle x(t, \xi)\rangle \tag{25}$$

is the expected value of the process at time t, and the wavelet coefficients are

$$d_k^{(j)}(t) = \int_0^1 x(t, M^{-1}(z))\psi_k^{(j)}(z)\,\mathrm{d}z, \tag{26}$$

$$= \int_a^b x(t, y)\Psi_k^{(j)}(y)\,\mathrm{d}M(y) = \langle x(t, \xi)\Psi_k^{(j)}(\xi)\rangle. \tag{27}$$

As for the PCE, the orthogonality of the Haar basis can be used to show that the variance of the process at each time is $\sum_{j=0}^{\infty}\sum_{k=0}^{2^j-1}(d_k^{(j)})^2$.

2.3.3. Evaluation of the Wiener–Haar coefficients

In practice, the resolution will be truncated to some finite $J = \max(j)$. Furthermore, most expansions will be for discrete stochastic processes (i.e., time series), so there is no harm in assuming that the stochastic process is a correlated random vector; i.e., time t belongs to a discrete index set. In this study, we also assume for simplicity that only a single continuous, uniformly distributed random variable is of interest; thus, we can write the process as $x(\xi)$ where the dimension, N, of x is equal to the number of time samples.

Under these conditions, the Wiener–Haar series, Eq. (21), can be written as

$$x(\xi) \approx x_0 + \sum_{j=0}^{J}\sum_{k=0}^{2^j-1} d_k^{(j)}\psi_k^{(j)}(\Pr(\xi)), \tag{28}$$

where $\{x, x_0, d_k^{(j)}\} \in \mathbb{R}^N$. The expansion coefficient vectors can be evaluated using the inner product relations defined above; i.e.,

$$d_k^{(j)} = \int_0^1 x(M^{-1}(z))\psi_k^{(j)}(z)\,\mathrm{d}z. \tag{29}$$

Because z is uniformly distributed on $[0, 1]$, Eq. (29) is the expected value of the integrand; that is,

$$d_k^{(j)} = \langle x\psi_k^{(j)}\rangle \approx \frac{1}{n}\sum_{i=1}^{n} x(M^{-1}(z_i))\psi_k^{(j)}(z_i) \tag{30}$$

for an ensemble of n time histories, each observed at N equally separated points in time. This expression is implemented below through standard MCS to generate the n realizations of the process.

Standard numerical integration methods might also be considered as candidates for evaluating $d_k^{(j)}$. This approach was explored using both the trapezoidal rule and Simpson's rule for comparison; however, like MCS, this approach is inefficient in practice because the current application requires a complete set of wavelet coefficients at each time step. We found that the convergence of the expansion coefficients from numerical integration was similar to those from MCS, so this approach will not be discussed further herein.

MCS and numerical quadrature both approach the evaluation of the coefficients as a projection operation that requires the computation of inner products. They do not take advantage of the potential efficiency embedded in the filter-based approach to the wavelet transform. Mallat's pyramid algorithm [15] for the discrete wavelet transform (DWT) is much quicker and, as will be demonstrated, yields Wiener–Haar coefficients that reproduce the process with significantly greater accuracy than MCS or numerical integration. The details of this algorithm are readily available in the standard wavelet literature, e.g., Burrus et al. [15] or Strang and Nguyen [24]. The DWT results presented herein are for $n = 2^{J+1}$ evenly spaced samples of

$z \in [0, 1]$. This restriction was imposed to simplify the implementation of the DWT algorithm by avoiding the need to compensate for boundary distortion that occurs when the signal's length is not a power of two [24,25]. Very localized boundary effects still remain in some of the results because no extension scheme was used, but this does not detract noticeably from the quality of the results.

3. Spectral Wiener expansions of a sinusoidal problem formulation

A model problem is examined next to demonstrate the poor large-time PCE convergence and to elicit its cause. The WHa expansion is employed to represent a sinusoidal stochastic process, $X(t) = \sin \omega(\xi)t$. The frequency is assumed to be a Gaussian random variable, $\omega = \omega_0 + \sigma_\omega \xi$, where ξ is a standard Gaussian random variable, $\omega_0 = 2\pi$, and the coefficient of variation (COV) is $\sigma_\omega/\omega_0 = 0.10$. Although a sinusoid with uniformly distributed random phase is a common textbook example (e.g., Ref. [20]), we were unable to locate a clear discussion of the more general non-stationary stochastic process described here; hence, we offer a detailed presentation of its features. The expansion coefficients, $\{\hat{x}_j(t)\}_{j=0}^{P}$, are approximated with a standard MCS of 1000 realizations, each containing 1000 time samples from $t = 0$ to 10. This time range includes 10 complete cycles at the mean frequency. The early evolution of the process is illustrated in Fig. 1, which overlays 50 realizations from $t = 0$ to 3.

With the specifications just given, two Hermite chaos expansions were generated, with $P = 6$ and 10 in Eq. (2). The resulting $\{\hat{x}_j(t)\}_{j=0}^{P}$ are shown in Figs. 2 and 3, respectively. Each $\hat{x}_j$ is oscillatory, but it is also localized in time because the spectral distribution of the energy in the random dimension shifts to higher polynomial chaoses (i.e., modes in the random dimension) as time progresses.

This non-stationary behavior is also evident in the probability density function (pdf) at various time slices, which are depicted in Fig. 4. These pdf are estimated from the original MCSs data; i.e., they do not yet reflect the projection onto the Hermite basis. At $t = 1$, the pdf is approximately symmetric about $x = 0$, but as time progresses, the pdf begins to appear stationary and develops peaks near $x = \pm 1$ with a valley around $x = 0$. This shape is reminiscent of the well-known distribution of a sinusoid with uniformly random phase between 0 and 2π [20].

A successful stochastic expansion of the sinusoidal random process ought to reproduce the non-stationary traits exhibited by the pdf in Fig. 4. The PCE produces a mean-square convergent representation of a second-

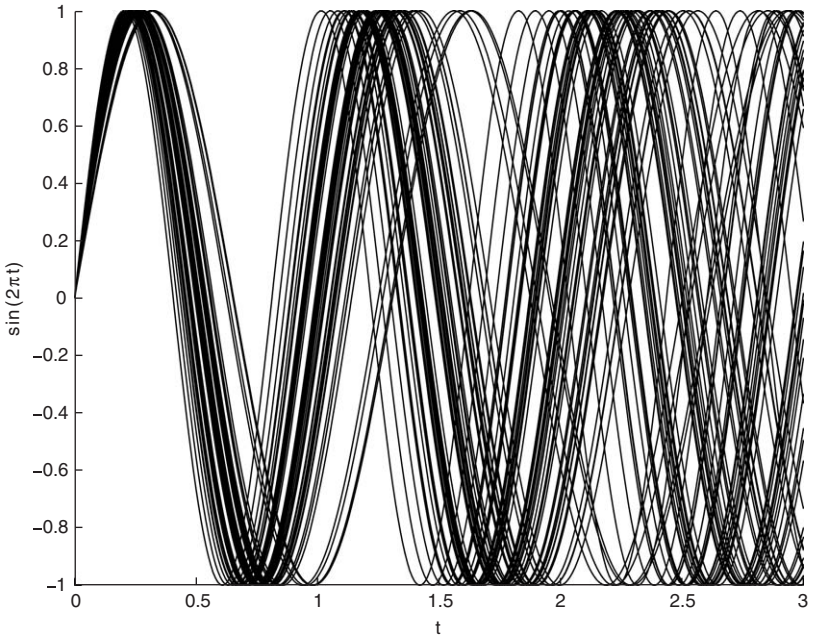

Fig. 1. Fifty realizations of the sinusoidal process with random frequency.

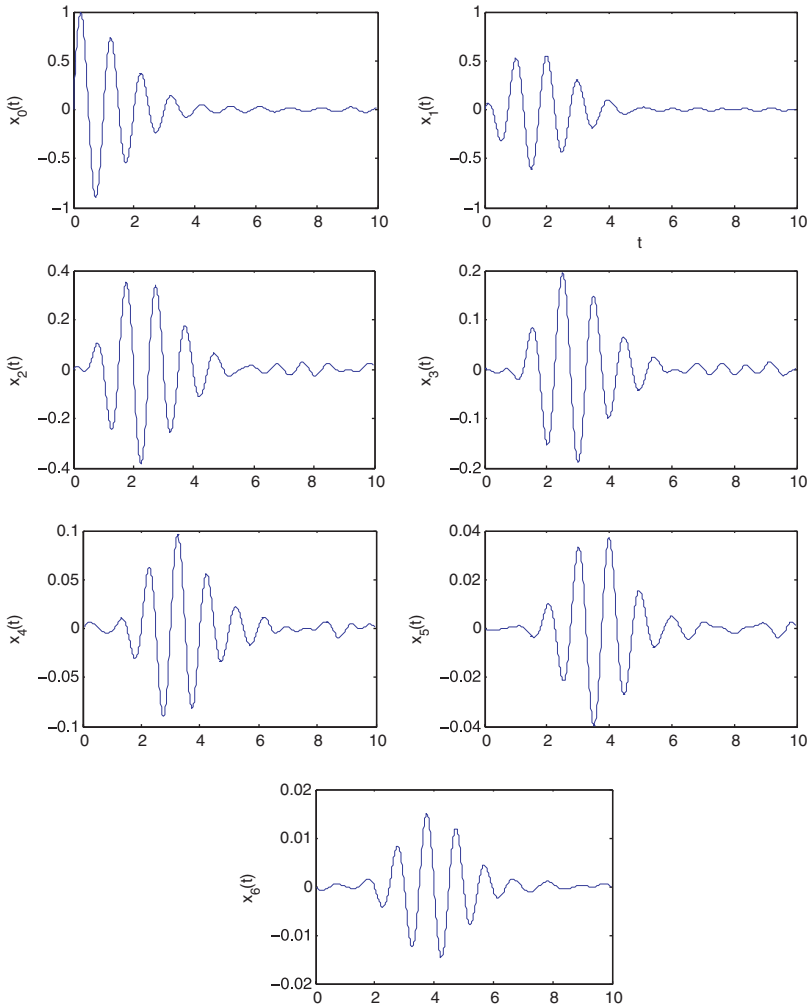

Fig. 2. Generalized Fourier coefficients for sixth-order polynomial chaos expansion of sine wave with random frequency. Vertical axes show $\langle x\mathrm{He}_j\rangle/\langle \mathrm{He}_j^2\rangle$ for each order j from 0 to 6.

order random process, but there is no guarantee that the expansion will converge equally quickly at each time. Furthermore, Li and Ghanem [26] observed that the PCE converges slowly for some nonlinear processes. We show herein that as time progresses, the increasing nonlinearity in the random dimension is responsible for the poor PCE convergence at large times.

3.1. Evolution of spectral Wiener expansions of the sinusoidal process

For the sinusoidal process, the shifting of energy to higher modes can be explained intuitively for the first few modes. This explanation is motivated by the visual evidence in Fig. 1. Consider the mean component ($\mathrm{He}_0 = 1$) first. Fig. 1 shows that for frequency variations that are small with respect to the mean frequency, the sinusoidal realizations remain highly correlated for about the first quarter-cycle; this is especially true during the initial time steps, when the evolution of the sinusoid is close to a linear function of its frequency. This translates initially to linear growth in $\hat{x}_0$ for $t<0.25$ approximately, whereas the other modes contribute almost nothing to this portion of the process. As time progresses, the frequency variations force the individual realizations to disperse so that $x(t)$ eventually becomes equally likely to be positive or negative at any time step; consequently, the mean term must approach zero. This occurs as a decaying oscillation at what appears

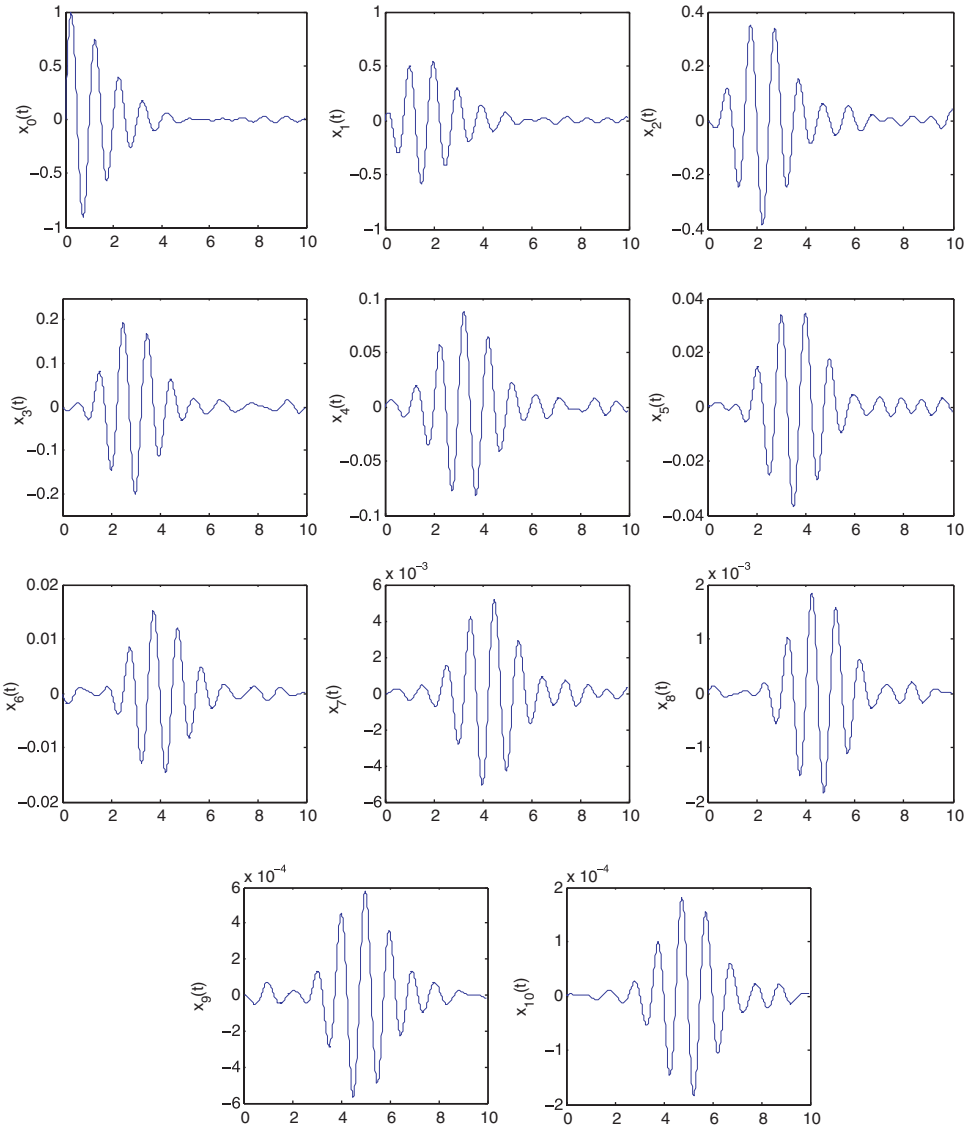

Fig. 3. Generalized Fourier coefficients for 10th-order polynomial chaos expansion of sine wave with random frequency. Vertical axes show $\langle x\mathrm{He}_j\rangle/\langle \mathrm{He}_j^2\rangle$ for each order j from 0 to 10.

to be the mean frequency of the process. This observation is corroborated by expanding $\sin\omega t$ for small changes in ω; i.e., $\sin\omega t = \sin(\omega_0 + \Delta\omega)t$ where $|\Delta\omega/\omega_0| \ll 1$. Taking the expected value of this for $\Delta\omega = \sigma_\omega\xi$ leads to

$$\langle \sin\omega t\rangle = \sin\omega_0 t\langle\cos\sigma_\omega\xi t\rangle + \cos\omega_0 t\langle\sin\sigma_\omega\xi t\rangle.$$

This expression can be simplified by recognizing that $\langle\sin\sigma_\omega\xi t\rangle$ is zero for all t if ξ is symmetric around zero. This can be seen directly by expanding $\sin\sigma_\omega\xi t$ in a Taylor series:

$$\sin\sigma_\omega\xi t = \sigma_\omega\xi t - \tfrac{1}{6}(\sigma_\omega\xi t)^3 + \tfrac{1}{30}(\sigma_\omega\xi t)^5 + \cdots .$$

For ξ symmetrically distributed around zero, $\langle\xi^{2k+1}\rangle = 0$ for all $k \in \mathbb{N}$. Enforcing this condition shows that $\langle\sin\sigma_\omega\xi t\rangle = 0$ for all t.

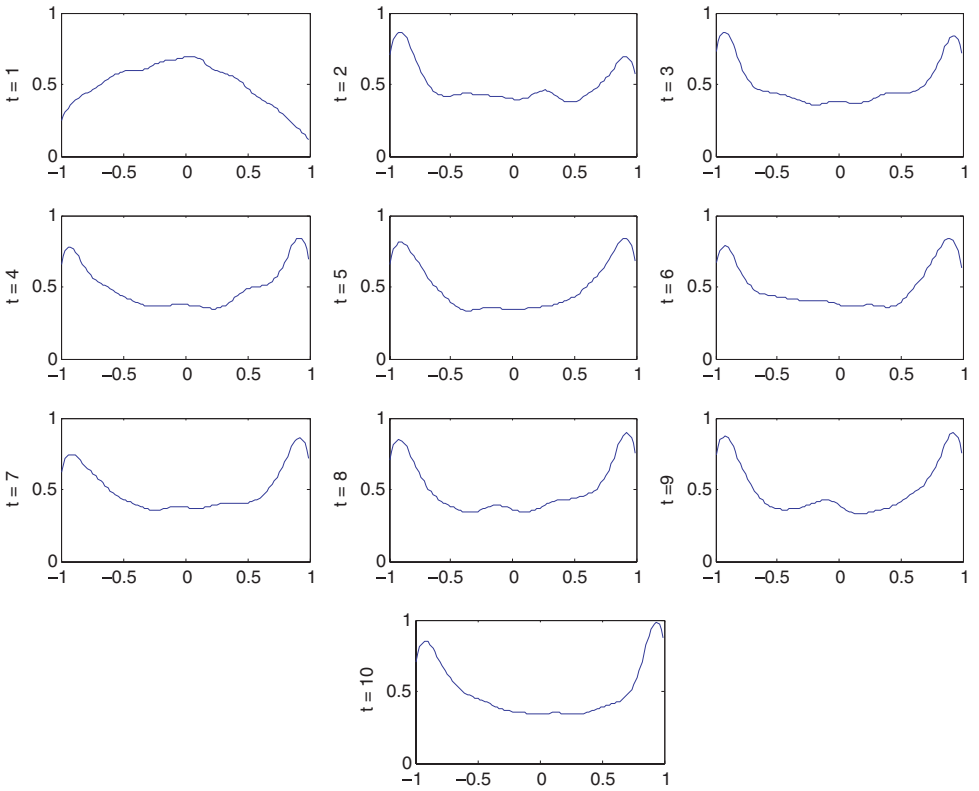

Fig. 4. Estimated probability density functions of $-1 \leqslant x(t) \leqslant 1$ at evenly-spaced time slices from $t = 1$ to 10. Ordinate label shows the time for which the pdf was computed. The pdf are based on the original Monte Carlo simulations, i.e., before the data are projected onto the polynomial chaos basis.

If we also expand $\cos \sigma_\omega \xi t$ in a Taylor series, recall that $\langle \xi^{2k} \rangle = 1$ for a uniform rv, and retain only the first three terms, we are left with

$$\langle \sin \omega t \rangle = [1 - \tfrac{1}{2}(\sigma_\omega t)^2 + \tfrac{1}{24}(\sigma_\omega t)^4 - \cdots] \sin \omega_0 t. \tag{31}$$

This approximate relation shows that $\langle \sin \omega t \rangle$ should decay at the mean frequency of the process for small t.

Fig. 4 shows that the pdf of x at $t = 1$ has a relatively broad central peak near $x = 0$, so the response is almost equally likely to be positive or negative by this time. The absolute value of the response is of course less than or equal to one, so the resulting pdf is qualitatively similar to a truncated Gaussian. Given that $\mathrm{He}_1 = \xi$, this observation accounts for the prominence of $\hat{x}_1$ for $1 \leqslant t \leqslant 3$. As noted above, this unimodal pdf is temporary and the process approaches a bimodal pdf for larger times; consequently, the first-order mode must also diminish over time.

For $t > 3$ (i.e., when multiple cycles have occurred), the randomness of ω causes ωt to be distributed more uniformly throughout the 2π interval, when the periodicity of $\sin \omega t$ is enforced; that is, further increasing the time value has little effect because the sine function is bounded and multi-valued. This explains the observed transition to stationary behavior similar to the sine function with random phase; in fact, this trend can be inferred from Fig. 1. Fig. 5, which shows the evolution of the standard deviation, suggests that the process is at least wide-sense stationary by $t = 3$; further examination of the density functions in Fig. 4 indicates that the process tends toward being stationary in the strict sense as well. Finally, note that the early oscillations in Fig. 5 occur at approximately twice the mean frequency of the process. This empirical result can be demonstrated analytically by expanding $\sin \omega t$ as before. The required algebra is too extensive to include here, but it leads to an expression of the form

$$\mathrm{Var}(\sin \omega t) \approx f_1(t) \sin^2 \omega_0 t + f_2(t) \cos^2 \omega_0 t,$$

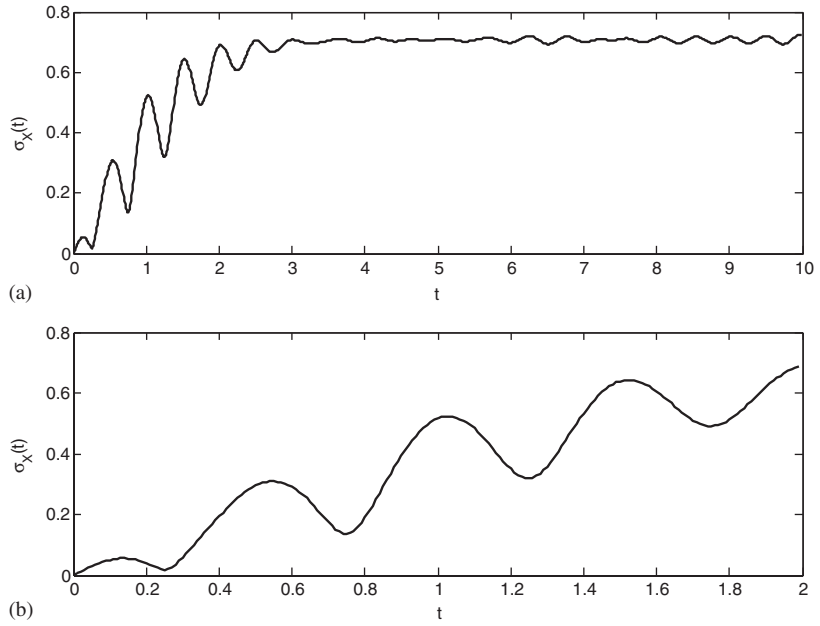

Fig. 5. (a) Standard deviation of the sinusoidal random process, as computed from the ensemble of 1000 realizations; (b) close-up view of (a) the first two dimensionless time units in (a).

where $f_1(t)$ is a fourth-order monomial in t and $f_2(t)$ is a sixth-order polynomial in t. The presence of the $\sin^2 \omega_0 t$ and $\cos^2 \omega_0 t$ terms accounts for the observed oscillation at approximately $2\omega_0$ in the standard deviation during its evolution.

3.2. Wiener–Hermite and Wiener–Legendre simulations of the sinusoidal process

The observed time-dependent behavior of the PCE coefficients has severe consequences for the time-accurate simulation of processes with periodic sample paths. Fig. 6 shows three realizations of the simulated process, each of which is based on Eq. (2) truncated at a particular value of P. Although the early oscillations appear similar to the original data, albeit with some surprisingly large amplitude variations between realizations (see Fig. 7), even relatively high-order expansions exhibit a characteristic decay at large times. In theory, the slow convergence can be compensated for by employing many more modes, but this is impractical. As Fig. 6 shows, a 14th-order expansion only delays the loss of energy. Results not presented here show that even a 20th-order expansion only delays the energy loss for approximately one more cycle. This indicates that the PCE is not well-suited for time-accurate simulation of essentially periodic processes. Short-time behavior is represented reasonably well by a low-order expansion, but economical expansions cannot be obtained for simulation runs longer than a few mean periods.

Similar characteristics were observed in WLa expansions of $\sin \omega(\xi)t$. In this case, ξ was assumed to be a uniform rv on $[-1, +1]$ and $\omega = 2\pi + \sigma_\omega \xi$. Values of $\mathrm{COV} = \sigma_\omega / 2\pi$ were assumed between 0.1 and 0.3 to examine the effect of the relative frequency range. $\mathrm{COV} = 0.1$ produced less severe but still noticeable large-time decay because the associated range of possible frequencies was smaller than in the Gaussian case. $\mathrm{COV} = 0.3$ produced a range of frequencies similar to those sampled from the Gaussian distribution, but with a higher likelihood of extreme frequencies. Many of the resulting WLa realizations were more erratic at large time values than their WHa counterparts; a small minority actually grew in amplitude. Fig. 8 shows these traits in realizations from a 10th-order WLa expansion.

An intuitive interpretation of the PCE coefficient properties is offered here. The severity of a function's nonlinearity with respect to its random input governs the required order of its PCE, with larger values of P needed for more nonlinear functions. This is a consequence of the fact that nonlinear processes can substantially distort the shape of an input pdf, so that the output distribution bears little resemblance to the

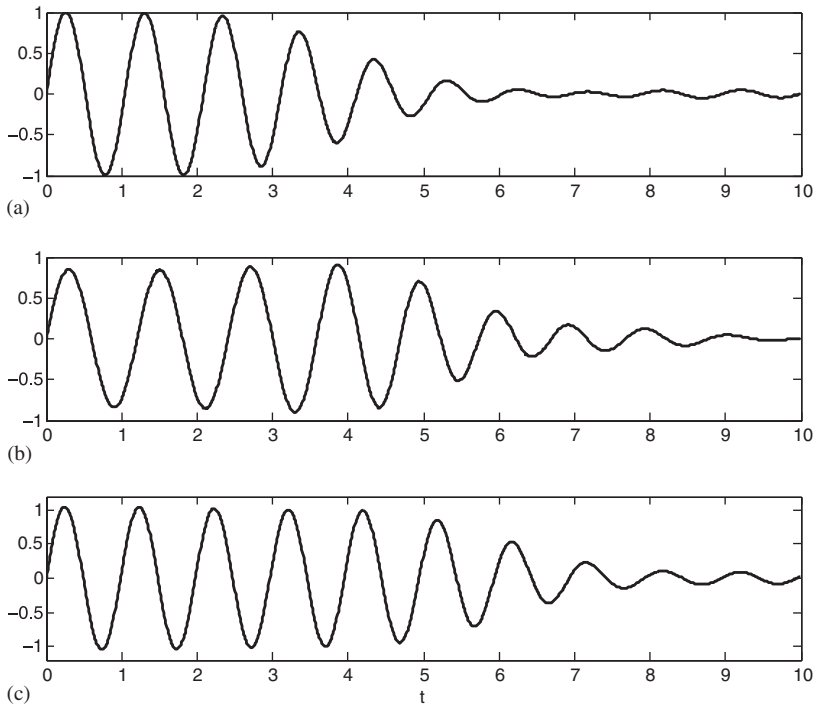

Fig. 6. Typical Wiener–Hermite realizations of the sinusoidal random process: (a) sixth-order expansion; (b) 10th expansion; (c) 14th-order expansion.

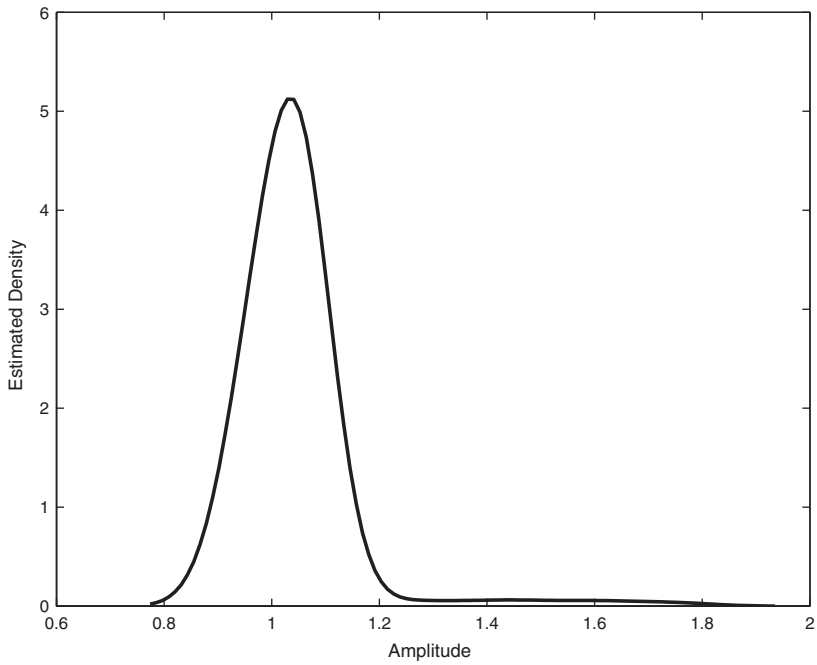

Fig. 7. Estimated density function for sample realizations from the 10th-order Wiener–Hermite expansions. Amplitude is taken as the maximum value for $t \leqslant 2$.

input distribution. The nonlinearity of the sine function is variable in that it increases with time; that is, the Taylor series of $\sin \omega t$ requires many terms to retain accuracy for a given ω when $\omega t \gg 2\pi$. Additional insight is gained by examining the nonlinearity of $x(t)$ versus ξ at a given time. Fig. 9 shows that it increases greatly with

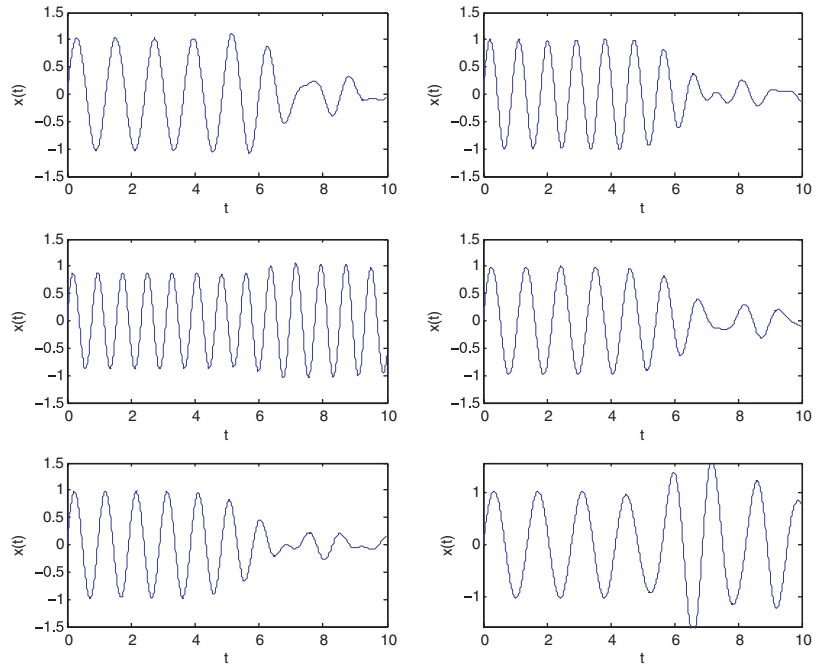

Fig. 8. Typical realizations of the sinusoidal random process for 10th-order Wiener–Legendre expansions.

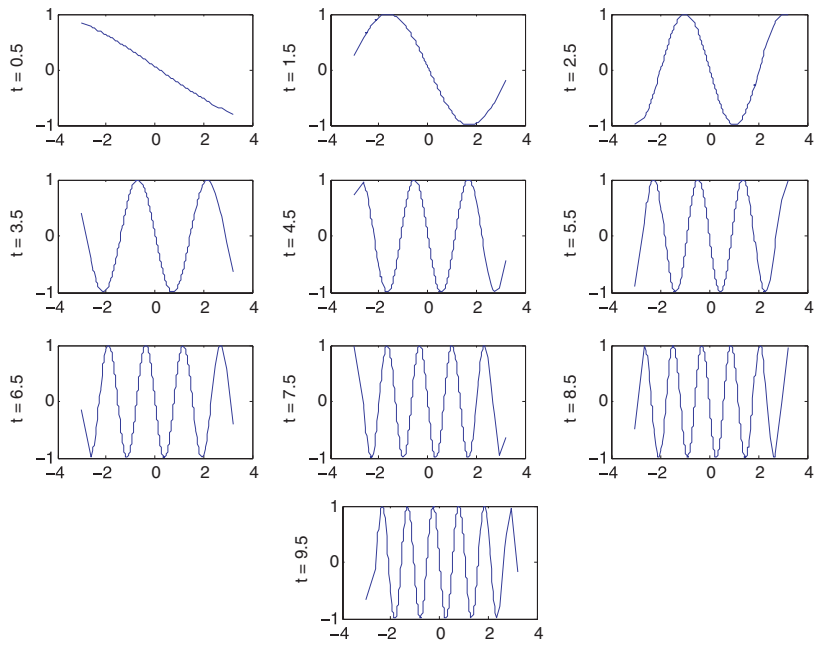

Fig. 9. Plots of $x(t)$ versus ξ at $t = 0.5, 1.5, \ldots, 9.5$, which show the increasing nonlinearity in the ξ-dimension as time progresses. Abscissa in each figure is ξ, with the range limited by the values generated in the Monte Carlo simulation. Ordinate in each figure is labeled with the corresponding time value.

time; consequently, a global polynomial fit like the truncated WHa expansion is unable to keep pace with the functional relationship between ξ and $x(t)$ as time progresses.

These observations indicate that the combined effects of the non-stationary argument, ωt, and the increasing nonlinearity of the sine function at large times demand an ever-increasing order of PCE to retain accuracy as time progresses. In this sense, although the expansion is guaranteed to be mean-square convergent in the random domain (i.e., ξ or $\omega(\xi)$), uniform convergence is not guaranteed for the PCE of $\sin \omega t$. Low-order terms are sufficient to reproduce the process for small times but even very high-order expansions are inadequate at large times.

4. Wiener–Haar expansion and simulation of the sinusoidal model problem

4.1. Background

The results presented above show that the failure of the PCE of the sinusoidal process at large times is induced by the increasingly nonlinear behavior of the process in the random dimension and the associated transition to a distinctly bimodal density function. Figs. 4 and 9 offer two perspectives on these properties. In Fig. 4, the nonlinearity and non-stationarity eventually map the Gaussian input pdf to an extremely bimodal pdf on a bounded domain. The changes in Fig. 9 were explained intuitively by comparison with the poor accuracy of the Taylor series of a sinusoid for large values of its argument.

These properties are difficult for a PCE to reproduce because of the global extent of the basis functions in the random dimension. The authors hypothesized that a wavelet expansion would be better suited to representing the complex random behavior of this process. The localization of behavior across multiple scales should permit the bimodal behavior observed in Fig. 4 and the associated increasing frequency in the random domain (Fig. 9) to be represented with sufficient accuracy.

This hypothesis was tested by employing the WHa expansion, as described in Eqs. (21)–(30). The frequency of the sinusoidal process was defined by $\omega = 2\pi + \sigma_\omega(z - 0.5)$, where z was uniformly distributed on $[0, 1]$. A COV of 0.6 was used instead of 0.1 to force the uniform random variable to include a range of values similar to the Gaussian and uniform variables employed in the WHa and WLa expansions, respectively.

4.2. WHa results and discussion

Three approaches to evaluating the WHa coefficients are considered:

(1) We first describe the characteristics exhibited by the MCS-based WHa expansion because MCS is commonly employed in non-intrusive Wiener expansions. MCS with 10,000, 20,000, and 40,000 realizations of the sinusoidal process was employed to evaluate statistical convergence. These sample sets clearly are much larger than the 1000 samples used for the WHa and WLa expansions. This is reasonable in that 1000 samples were more than sufficient to demonstrate the fundamental handicap of spectral expansions for oscillatory random processes, whereas the large sample sets are employed for WHa only to examine the statistical convergence of the non-intrusive multiresolution expansion. Section 4.2.1 contains an extensive discussion of the MCS results, and an attempt is made to equitably compare WHa and WHa expansions with similar truncation levels. For each of the MCS ensembles, the WHa expansion was truncated to either $J = 5$ or 6. Including the single lowest approximation (i.e., mean or scaling function) level, this required the estimation of 2^{J+1} expansion coefficients at each time step with 2^J coefficients at the finest resolution. Consequently, even moderate WHa expansions required the computation of more coefficients than normally are computed in stochastic projections.

(2) Numerical integration with Simpson's rule was applied to a uniformly spaced discretization of $z \in [0, 1]$. This approach works, but we do not discuss this approach further because it offers no clear computational advantage over MCS when there are substantial oscillations in the random dimension.

(3) The MCS ensembles mentioned above are much larger than can be hoped for in simulating complex nonlinear systems. The results described in Section 4.2.2 show that the DWT or filter-based approach offers substantial advantages over MCS for efficiently evaluating the WHa coefficients and simulating the

process with many fewer samples. Mallat's algorithm was used to compute the DWT with $n = 2^{J+1}$ evenly spaced values of z. The DWT results were computed for $J = 7$ or 256 samples. Comparison with lower truncation levels, e.g., $J = 6$, from the MCS results is straightforward because the pyramid algorithm can be reversed to efficiently reconstruct the process at any coarser scale.

4.2.1. MCS-based expansion coefficients

Fig. 10 shows three realizations selected at random from the WHa expansion for $J = 5$ and 10,000 MCS realizations. Comparison with the Wiener–Hermite realizations in Fig. 6 shows that the energy loss at large times appears to have been eliminated, but the amplitude of the simulations is still a random function of z instead of one exactly. Close examination of a phase plane plot (not shown here) for one of the realizations reveals a very slight, smooth decay of approximately 1.5% over the full duration for $J = 5$; the decay for $J = 6$ is closer to 0.5%, but it is still measurable. Because these decay rates are relatively low, the WHa amplitude is defined herein as the maximum value observed during a given realization. Fig. 11, shows the estimated density functions of the amplitude from 1000 simulated realizations based on the $J = 5$ WHa expansion. The variance decreases as the size of the original set of realizations increases from 10,000 to 40,000, but it is still larger than desired.

A brief convergence study (see Table 1) was performed to examine the influence of the original ensemble size and the expansion order on the statistics produced by the associated WHa expansion. Statistics were computed from 1000 simulated realizations for each case. The mean amplitude of each set is close to the others, but the estimated range and standard deviation definitely decrease with increasing sample size of the original set.

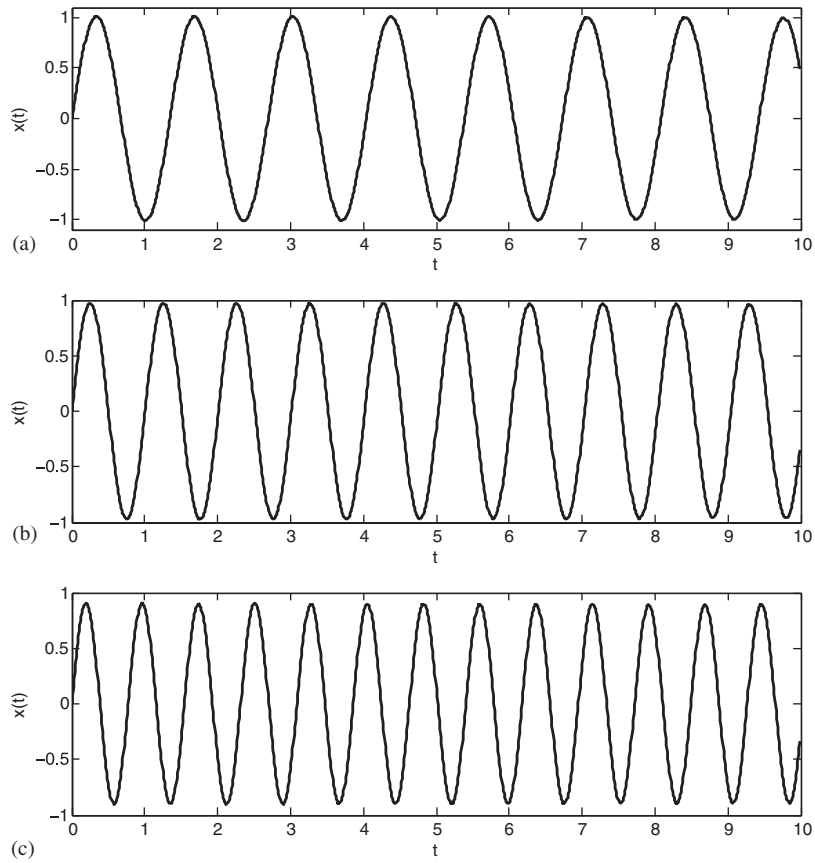

Fig. 10. Three sample realizations of the sinusoidal random process for the Wiener–Haar expansion for $J = 5$; (a) lowest frequency used in the simulation; (b) middle frequency; (c) highest frequency.

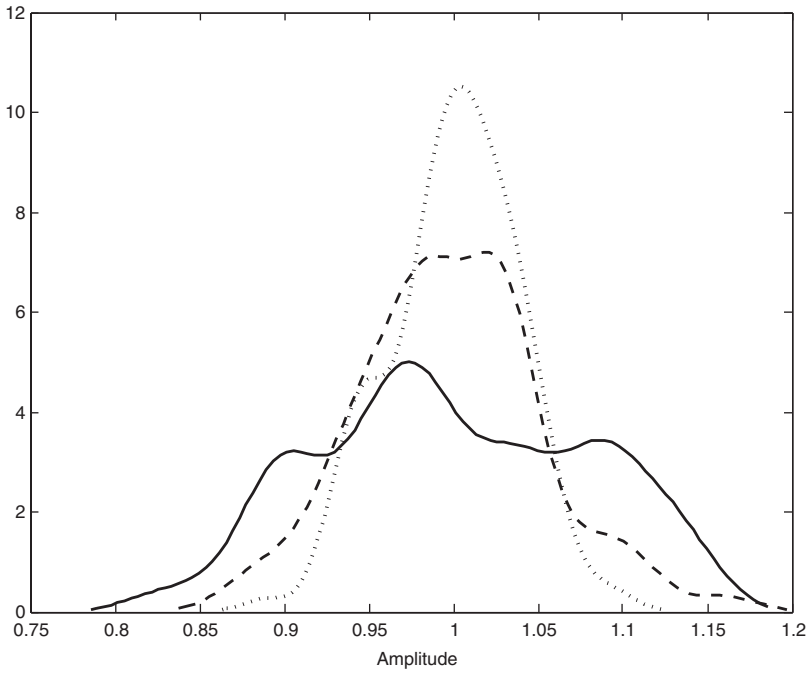

Fig. 11. Estimated amplitude density function of the sinusoidal random process, as simulated by the Wiener–Haar expansion with $J = 5$. Expansion coefficients computed through Monte Carlo simulation. Amplitude is defined to be the maximum value observed during a time history. See the accompanying text for discussion. — 10,000 realizations, - - - 20,000 realizations, ··· 40,000 realizations.

Table 1
Amplitude statistics for Wiener–Haar simulation of sinusoidal process

J	Input realizations	Min	Max	Mean	Std. dev
5	10,000	0.8256	1.1455	1.0001	0.0792
	20,000	0.8734	1.1612	0.9983	0.0539
	40,000	0.8895	1.0973	1.0003	0.0374
6	10,000	0.7549	1.3311	1.0073	0.1181
	20,000	0.7488	1.1274	1.0022	0.0856
	40,000	0.8351	1.1584	0.9973	0.0619

Wiener–Haar expansion coefficients generated through Monte Carlo simulation.

However, the amplitude variance increases with the order of the expansion, J, or resolution level, so that a larger initial ensemble is required for estimating the higher-order expansion coefficients if the resulting variance is to be maintained. This also is reflected in Fig. 12, which is the Wiener–Haar equivalent of the $t = 9$ frame in Fig. 9. The $J = 6$ curve exhibits oscillations around the peaks that are not present in the original data, which is purely sinusoidal in ξ for any t. These peak oscillations exist in the MCS results, but not in the DWT results described below. They occur because, as shown in Fig. 12, the higher truncation level pulls in wavelets whose support is much less than the wavelength of the original data. As shown below, these piecewise-constant wavelets have substantial secondary components at high frequencies and correspondingly short wavelengths. Hence, the resulting coefficients become sensitive to local variations in the sampling density. A larger initial ensemble should suppress this behavior, but as noted above, it is unlikely that such a large ensemble will be available in practical applications.

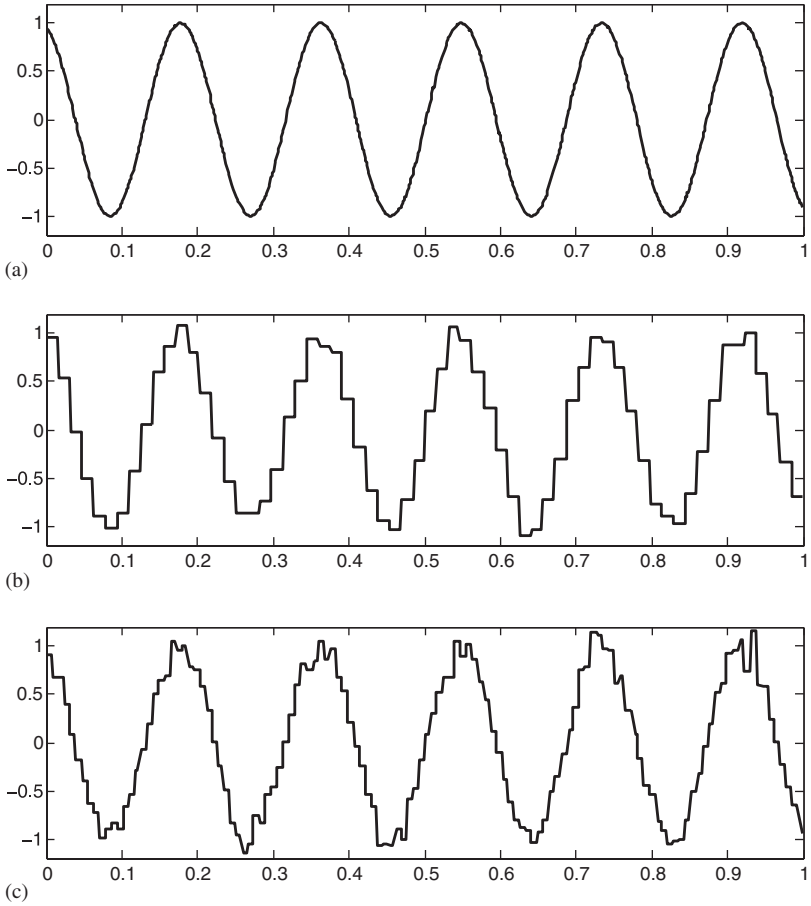

Fig. 12. Observed values of the sinusoidal process at $t = 9$ plotted against the associated value of the standard uniform random variable: (a) original data; (b) MCS-based Wiener–Haar simulation with $J = 5$; (c) MCS-based Wiener–Haar expansion with $J = 6$.

These observations quantify the trend already seen in Fig. 11 and indicate that the size of the original ensemble strongly affects the convergence of the wavelet coefficients that encode the second and perhaps higher moments. This implies that the amplitude variation produced by the WHa expansion is a consequence of the both the truncation (i.e., resolution) level and the inherent variation in an MCS. Relatively slow convergence of the WHa expansion was also observed by Le Maître et al. [16] in their application to bifurcations of stochastic systems.

Interesting characteristics were also elicited by studying a WHa expansion with much coarser resolution, $J = 3$. The amplitude variance continued to decrease with the resolution level, so that the observed amplitudes were generally more closely packed than for $J = 5$ or 6. However, Fig. 13 shows that this resolution scale was insufficient to maintain time accuracy because the decay observed in the spectral expansions reappeared, although in a less severe form. The decay is noticeable but compares favorably with the 14th-order WHa realizations (see the bottom frame of Fig. 6), which had a similar number of coefficients in the expansion (16 for WHa versus 15 for WHa). Moreover, the variance of the observed amplitudes before decay was much smaller than those observed for WHa (e.g., Fig. 7 for $P = 10$). The eventual decay in the $J = 3$ WHa simulations is caused by the inability of the coarse Haar wavelets to resolve the higher frequency oscillations in the random dimension.

The kernel density estimators for the amplitude (Fig. 11) also obscure an important detail. The WHa simulated amplitudes are actually constrained to a discrete set, with the number of admissible value limited by the number of wavelets at the finest resolution scale. Fig. 14 vividly illustrates this by showing the observed

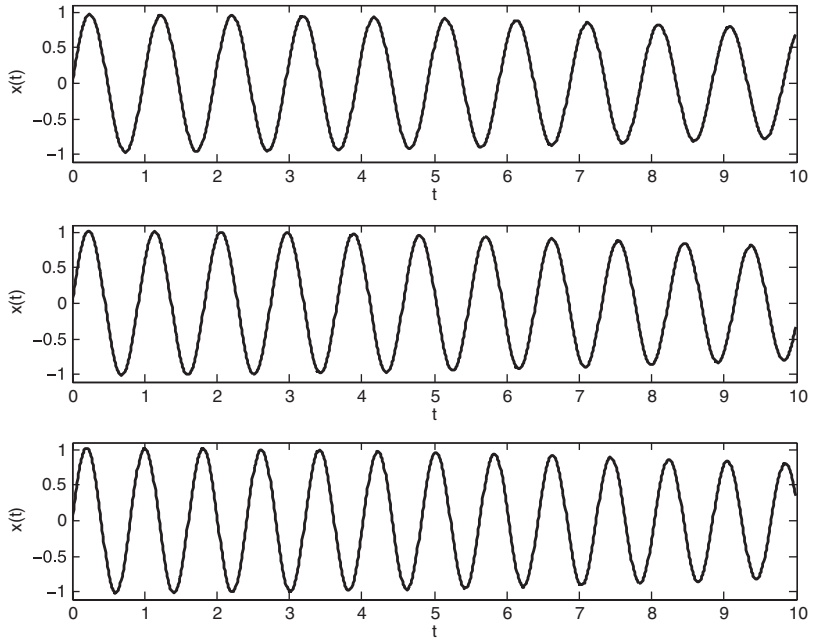

Fig. 13. Three sample realizations of the sinusoidal random process for the Wiener–Haar expansion for $J = 3$.

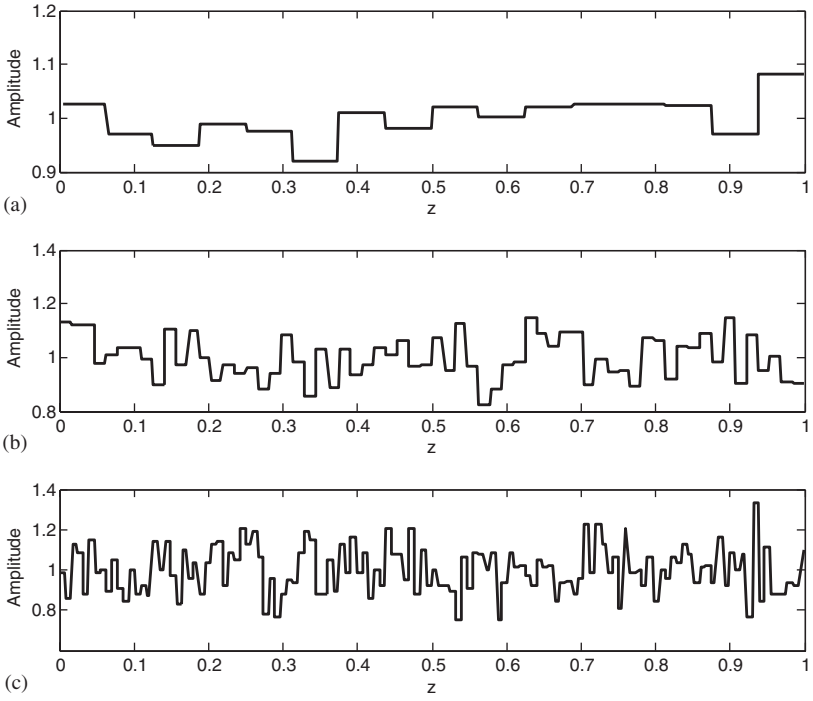

Fig. 14. Observed amplitudes in the simulated sine realizations as a function of z: (a) $J = 3$; (b) $J = 5$; (c) $J = 6$.

amplitudes for $J = \{3, 5, 6\}$ as a function of $z \in [0, 1]$. This should be expected because the Haar series divides the range of rv z into a set of disjoint intervals (i.e., a partition) such that each basis function is either 0 or ± 1 on a given interval. The finest division is $\Delta z = 1/2^J$, so the simulated process value at any given time is

determined by the particular half of the interval $[k, k+1]\Delta z$, $k \in \{0, \ldots, 2^J - 1\}$ in which the sampled value of z falls; other realizations of z can only be distinguished if they fall into separate resolution intervals.

The almost complete elimination of energy loss at large simulation times is a substantial improvement over the WHa and WLa results. The ultimate source of this improvement lies in the ability of the wavelet basis to capture localized behavior in the random dimension. Examination of the simulated density functions from several time slices showed good reproduction of those from the original process (Fig. 4). This indicates that the WHa expansion can indeed capture a wide range of probability distributions in a strongly non-stationary process.

The non-stationary nature of the process is again reflected in the time dependence of the WHa expansion coefficients. Fig. 15 shows the coefficient time histories for the scaling function and the coarser scales in the WHa expansion for $J = 6$. These are plotted through $t = 20$ instead of $t = 10$ for to illustrate the re-appearance of lower scales as time progresses. This effect is discussed below.

Because the individual resolution scales are orthogonal in a MRA, the coefficients presented here are, except for sampling variation, the same as those computed for $J = 3$ and 5. The time dependence of the mean value is captured in the scaling function coefficient (top frame of Fig. 15), which is similar to the first frame in Figs. 2 and 3. The first wavelet scale ($j = 0$) is complementary to the scaling function in that when one of these is zero,

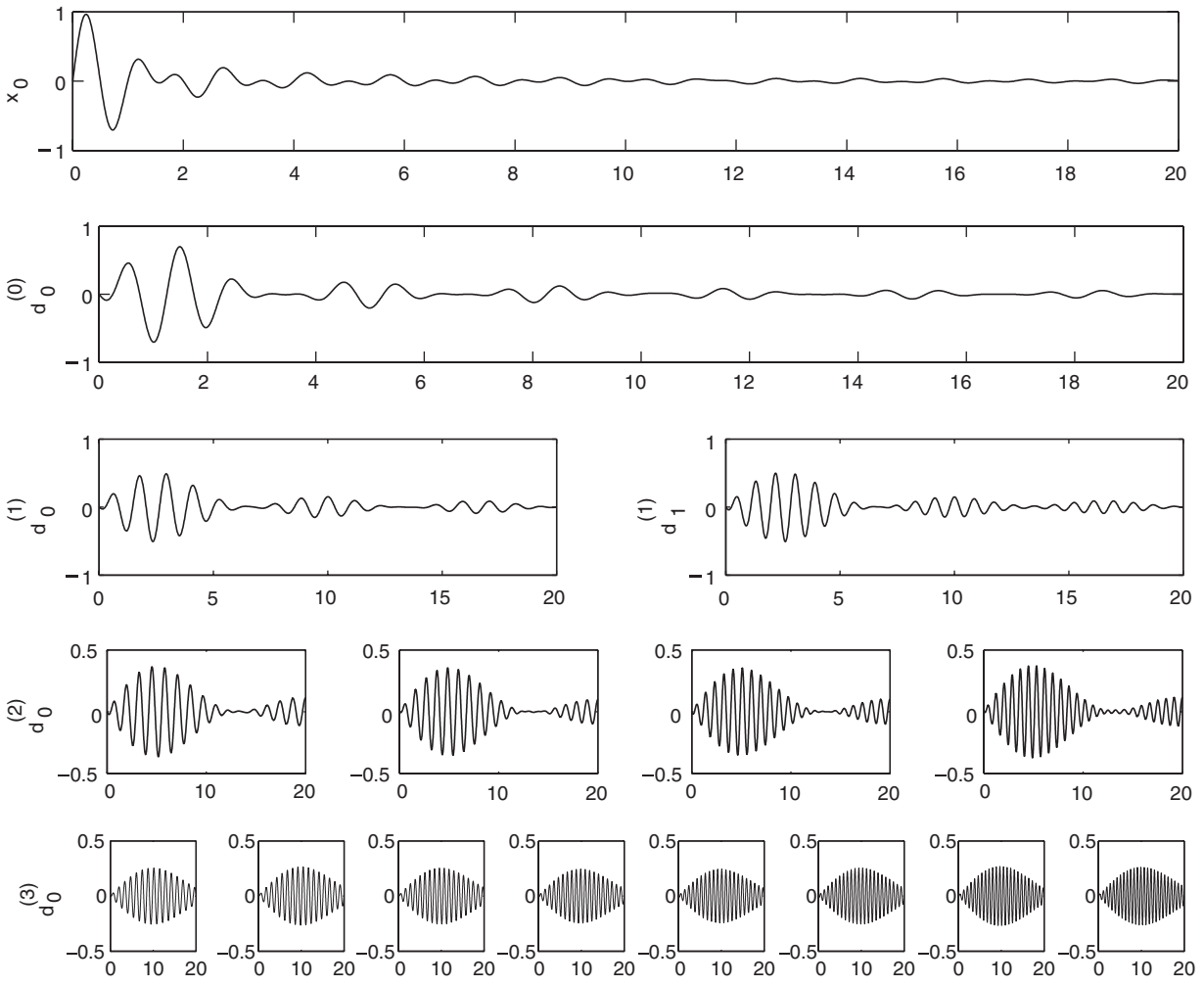

Fig. 15. Wiener–Haar expansion coefficients for the sinusoidal random process through $t = 20$. The top frame is the time history of the scaling function coefficient, $x_0(t)$; the second row shows the coarsest wavelet scale, $d_0^{(0)}(t)$, and succeeding rows show progressively finer scales. These plots were taken from the WHa expansion for $J = 6$; the three finest scales are not shown.

the other is either at an extremum or also zero; this follows from the orthogonality of $\phi(z)$ and $\psi_0(z)$. The $j = 1$ and 2 coefficients grow and decay much like the WHa coefficients (Figs. 2 and 3), and the $j = 3$ coefficients grow over time to reflect the increasing oscillation frequency in the random dimension, which was illustrated in Fig. 9 for the normally distributed frequency. The dominance of the higher scales at large times is driven by the large pdf peaks near $x = \pm 1$ (see Fig. 4), which can be synthesized only by the finer scale wavelets.

The re-growth of the $\psi^{(1)}$ components around $t = 8$ is associated with the multiple frequencies contained in each Haar basis functions. The Fourier transform of the mother wavelet can be written as [23]

$$\widehat{\psi^{(0)}}(v) = \int_{-\infty}^{\infty} \psi^{(0)}(z) e^{-2\pi i v z}\, dt = i e^{i\pi v}\left(\frac{1-\cos \pi v}{\pi v}\right). \tag{32}$$

It follows that

$$\widehat{\psi_k^{(j)}}(v) = 2^{-j/2} e^{\frac{-2\pi i k v}{2^j}} \widehat{\psi^{(0)}}\left(\frac{v}{2^j}\right), \tag{33}$$

where v is the frequency in the z-dimension (see Fig. 16); hence, $|\widehat{\psi_k^{(j)}}(v)|$ oscillates and decays with increasing frequency. As $\omega(z)t$ grows over time, the z-dimension oscillations gradually move into and out of correlation with Haar wavelets whose fundamental wavelengths are longer than that of the process at a given time. This effect is illustrated in Fig. 15, which shows the coefficients for a process with twice the original duration and the same distribution parameters as Fig. 15. The longer-scale components experience multiple growth and decay periods as time passes and the individual modes of each wavelet are excited. The decay of $|\widehat{\psi_k^{(j)}}(v)|$ with increasing v is reflected in the lower amplitude of each succeeding high-correlation phase in the associated $d_k^{(j)}$. This behavior does not noticeably affect the simulation quality, which continues to exhibit a very slight, smooth temporal decay.

An interesting characteristic of the coefficient time histories is the increase in their frequency as k, the translation parameter, increases in a given scale. This is clear even in $d_1^{(1)}$, which oscillates more rapidly than $d_0^{(1)}$, and the trend continues for higher scales. As k, the translation parameter, increases with j fixed, $\psi_k^{(j)}(z)$ becomes centered on a higher value of z, which in turn isolates a higher frequency, $\omega(z) = 2\pi + \sigma_\omega(z - 0.5)$. The result is that each wavelet coefficient oscillates in time at the frequency around which it is centered and grows or decays to reflect the relative importance of the scale it represents in the random dimension; these are

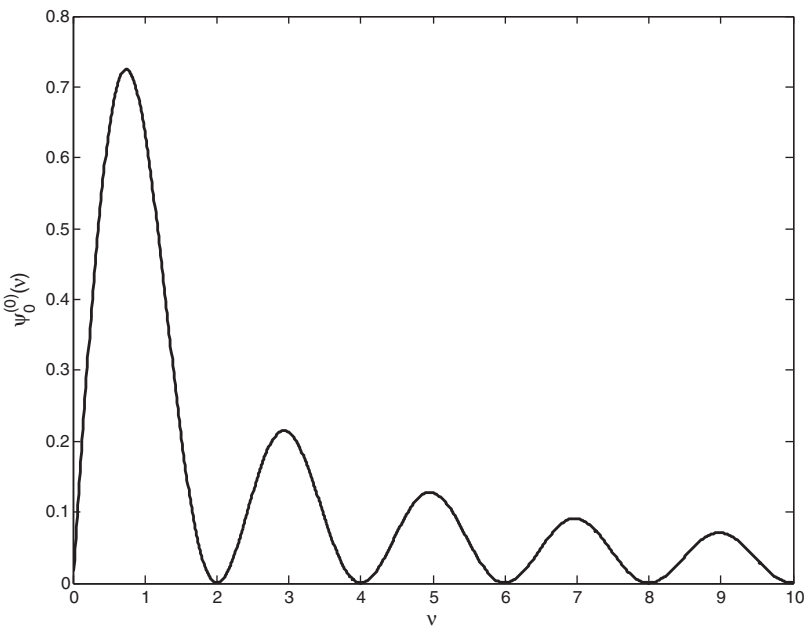

Fig. 16. Absolute value of the Fourier transform of the Haar mother wavelet.

the scales present in the time slices shown in Fig. 9. Increasing the resolution of the WHa expansion permits it to encode a more finely discretized set of temporal frequencies while simultaneously providing the ability to capture higher frequencies or more irregularity in the random dimension. It is this combination of traits that enables the WHa expansion to represent the sinusoidal stochastic process more effectively than the global bases of the WHa and WLa expansions.

4.2.2. *WHa coefficients from Mallat's pyramid algorithm*

As noted above, only 256 evenly-spaced samples were needed to compute the $J = 7$ WHa expansion through Mallat's pyramid algorithm. Fig. 17 shows the great increase in accuracy of the WHa expansion when Mallat's algorithm for the DWT is used to compute the coefficients instead of MCS or numerical integration. In particular, the bottom left frame of this figure, which is for $t = 9$, should be compared with the $J = 5$ frame in Fig. 12. The current approach for evaluating the projections tracks the oscillations in the random dimension with much greater consistency than MCS. Each plot in Fig. 17 actually shows the WHa simulations overlaid on the original data. Except for the piecewise nature of the WHa plots, the curves are almost indistinguishable.

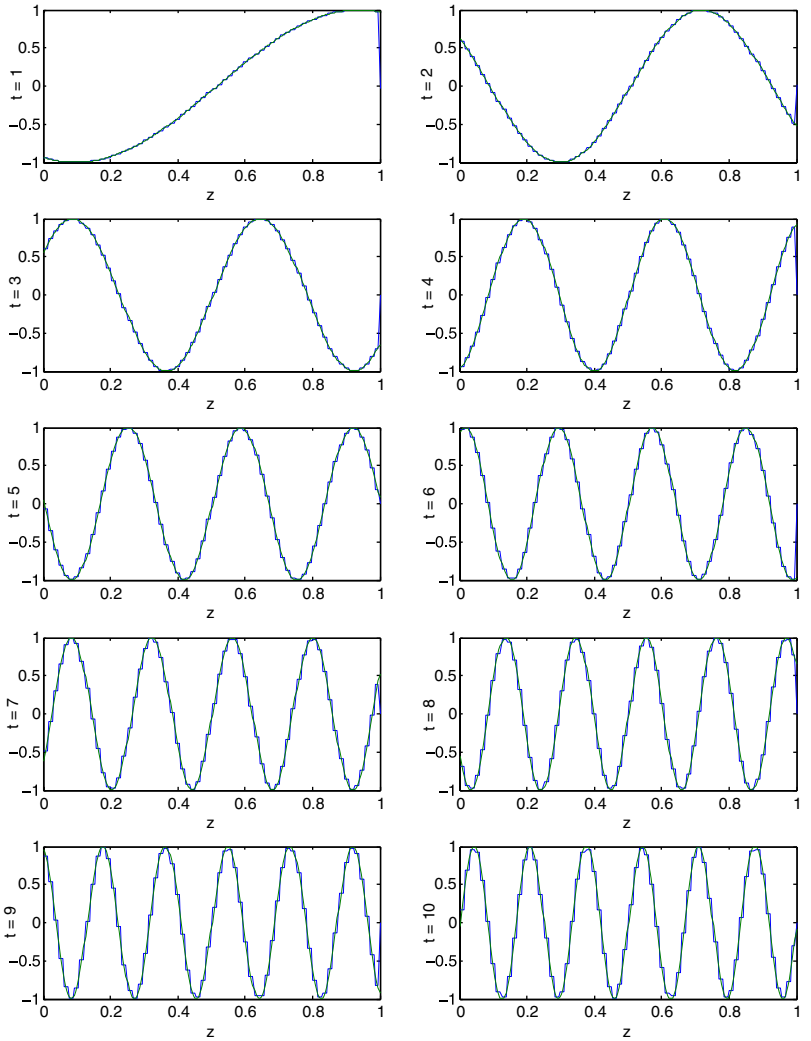

Fig. 17. Observed values of the sinusoidal process at $t = \{1, \ldots, 10\}$ plotted against the associated value of the uniform random variable, $0 \leqslant z \leqslant 1$. The piecewise constant curves are from the $J = 5$ Wiener–Haar expansion in which Mallat's algorithm is used instead of Monte Carlo simulation to estimate the expansion coefficients. The top left frame is for $t = 1$ and the bottom right frame is for $t = 10$, the final time step.

Higher truncation levels are not shown simply because they cannot be visually distinguished from the exact results without great magnification. The only noticeable discrepancy between the simulated and original process in this case is a localized boundary distortion, which is almost imperceptible in Fig. 17 near $z = 1$. This distortion might be mitigated by standard methods, such as periodic or symmetric extension of the data. Aside from the boundary distortion and numerical errors due to finite precision arithmetic, the Mallat-based WHa expansion yields perfect reconstruction of the original data, so that no significant variation occurs in the simulated amplitude of the sinusoid.

Not only does the Mallat-based WHa expansion produce much higher accuracy for a given number of samples than the MCS and numerical integration approaches, it does so with much greater computational speed. No formal timing study was performed, but the inherent efficiency of the pyramid algorithm is reflected in the well-known result that it is an $O(n)$ process when the quantity of data being transformed is a power of two [25]; therefore, the DWT-based WHa expansions demonstrated herein require $O(n)$ operations at each time step to compute all of the expansion coefficients. In contrast, MCS and numerical quadrature are $O(n)$ for each individual coefficient (e.g., see Eq. (30)), or $O(2^{J+1}n)$ for all of the coefficients at each time step.

Fig. 17 also emphasizes again the periodic nature of the sinusoidal process in the random dimension. As noted in Section 1, Millman et al. [14] employed a spectral Wiener expansion with a Fourier basis to compensate for the failure of the Hermite basis functions to properly reproduce limit cycles in a simple aeroelastic model problem. The apparent utility of this approach seems to be corroborated by the obvious periodicity in Fig. 17. However, the primary aspect of a nonlinear system that exhibit limit cycles is not the limit cycles themselves but the Hopf bifurcation that produce these limit cycles, in particular when the bifurcation is subcritical. In this regard the WHa expansion should be far superior to the Fourier-based chaos expansion. This is because, as demonstrated in the next section, the subcritical bifurcation appears as a step discontinuity in random dimension; see Figs. 21 and 23 for examples. This discontinuity should present a difficult convergence problem for the Fourier chaos expansion, just as a step leads to poor local convergence for a traditional Fourier series expansion in time or space. Results presented in the next section show that the WHa expansion incorporates the step discontinuity with little difficulty.

5. Wiener–Haar expansion of an elementary nonlinear system

The WHa expansion has been shown to successfully capture the fundamental traits of the sinusoidal model problem. A logical intermediate step before extending it to computationally expensive aeroelastic problems is to study its performance with a more elementary nonlinear system that undergoes a Hopf bifurcation. We employ a generalization of a simple model that exhibits a subcritical Hopf bifurcation, as described by Strogatz [27]. The governing equations are:

$$\dot{x} = c_1 x + c_2 y + c_3 xy + c_4 x^5, \tag{34}$$

$$\dot{y} = c_5 x + c_6 y + c_7 y^3 + c_8 y^5. \tag{35}$$

The fifth-order terms were added Strogarz's example to restrain the oscillation amplitude and thereby induce a limit cycle after the bifurcation occurs. In the results described here, $c_1 = c_6$ is the bifurcation parameter, which is set at -0.2. Parameter c_7 is modeled as a uniform random variable between 0.5 and 1.0, so that its mean or baseline value is 0.75. This parameter was chosen to be random because it plays a role similar to nonlinear stiffness terms in certain canonical aeroelastic systems (e.g., see the recent papers by Pettit and Beran [3,4]). The other parameters are fixed at $c_2 = -1$, $c_3 = 1$, $c_4 = c_8 = -0.25$ and $c_5 = 1$. The initial conditions are fixed at $x(0) = y(0) = 0.6$.

The system was numerically integrated with the *ode23* algorithm in Matlab 7. Results were generated for $0 \leqslant t \leqslant 100$ with a specified time step of $\Delta t = 0.01$, so that 10,001 time samples were computed for each realization. Fig. 18 shows a typical limit cycle for this system. Numerical experimentation shows that the occurrence and amplitude of limit cycles for this system is sensitive to parameter c_7 and the initial conditions, but only randomness in c_7 was studied.

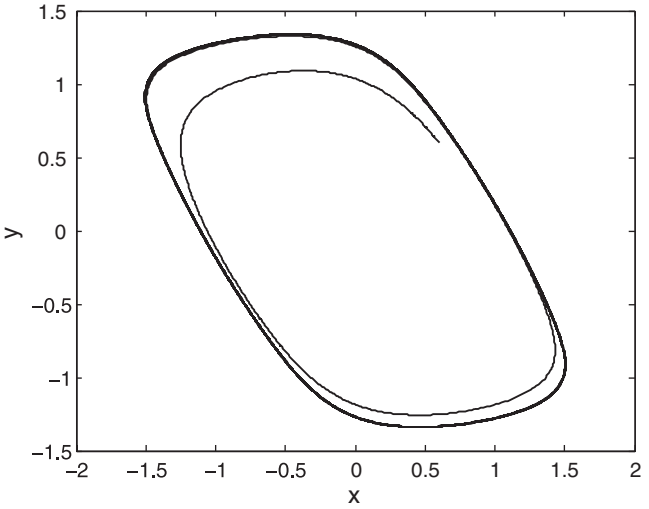

Fig. 18. Limit cycle in the baseline nonlinear model problem, i.e., with the random parameter $c_7 = 0.75$.

5.1. Stochastic analysis and simulation of the nonlinear model problem

Mallat's DWT algorithm was used to evaluate the time-dependent WHa expansion coefficients because of its superior speed and resolution convergence. As noted above, only c_7 was allowed to be random; i.e., $c_7(z) = 0.5 + 0.5z$, where z is uniformly distributed on $[0, 1]$. The range of variation was chosen so that both decaying oscillations and limit cycles would occur. An ensemble of 256 realizations, each with 10,001 evenly spaced samples for $0 \leqslant t \leqslant 100$, was generated at evenly spaced values of z to facilitate easy implementation of the DWT. As for the sinusoidal problem, no effort was made avoid boundary effects in the DWT. Using the notation defined above, $n = 256$ realizations corresponds to a maximum resolution level $J = 7$.

Figs. 19 and 20 illustrate the $J = 5$ WHa simulation for $z = 0.682$ and 0.780, respectively. These values were selected because they typify the best and worst levels of expansion accuracy. The phase plane plots show that the truncated WHa expansion captures the essence of the long-term dynamics, but the time histories, $x(t)$, show that the expansion error at a given time,

$$\varepsilon(t, z) = x_{\text{approx}}(t, z) - x(t, z) \tag{36}$$

can be small (Fig. 19(c)) or large (Fig. 20(c)). If the goal of the simulation were to determine the likelihood of limit cycles developing, this variability in time accuracy might be tolerated; however, time accurate simulations certainly would require more terms to be retained in the expansion.

Two long-term response quantities are presented to demonstrate the general efficacy of the WHa analysis and reduced resolution simulations across the full range of random parameter values: the simulated values of $x(t, z)$ at $t = 90.00$ and the maximum value of $|x|$ for $t > 80$. The second metric was chosen to allow the system sufficient time to either achieve a converged limit cycle or decay to zero response. The alloted time interval is sufficient to ensure that the post-bifurcation realizations complete at least a full limit cycle before the long-term amplitude is recorded. The WHa-based simulations discussed herein include 256 MCSs based on sample of c_7. Only simulations at wavelet resolution levels $J = 4$ and 5 are presented to illustrate the convergence of the multiresolution-based expansions. The two highest resolutions, $J = 6$ and 7, are not shown because, other than in the neighborhood around $z = 0.3$, they are practically indistinguishable from the original data at normal magnification.

Fig. 21 compares simulations to the original data at $t = 90.00$. The WHa expansion easily localizes oscillations and sharp changes in the random dimension. The nonlinear sensitivity to $c_7(z)$ is quite evident in the sudden appearance of substantial response for z close to 0.3. The primary shortcoming of the WHa expansion is the piecewise constant nature of the Haar basis functions, which are not well suited to precisely

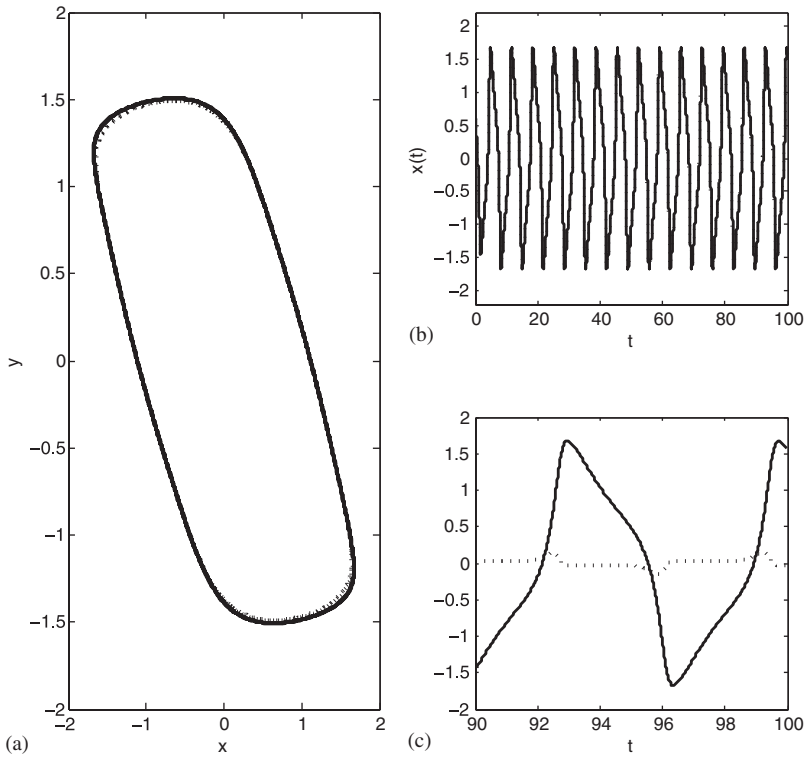

Fig. 19. Comparison of full model and $J = 5$ Wiener–Haar simulation for $z = 0.682$ or $c_7(z) = 0.841$: (a) phase plane plot of limit cycle; — full model, ⋯, Wiener–Haar; (b) $x(t)$; — full model, ⋯, Wiener–Haar; (c) close-up of (b) for full model, —, with overlay of expansion error, ⋯ .

tracking smooth variations. However, this trait is acceptable when weighed against the substantial improvement in the long-term accuracy over chaos expansions with global basis function. Future work should explore using a more general MRA to improve the tracking of smooth features.

An alternate view of the simulated response at $t = 90.00$ is provided by Fig. 22, which shows the estimated density functions for $J = 4$ and 5. The tails of these distributions exceed the actual range of sampled response values because of the finite kernel width employed in generating the estimated densities. Nevertheless, a small but noticeable consequence of the reduced resolution is the truncation of the tails as extrema of the oscillations in the random dimension (Fig. 21) are chopped off by the larger scales in the truncated Haar basis.

The maximum value of $|x|$ for $t > 80$ is depicted in Fig. 23 for the same values of $c_7(z)$ and resolution levels in Fig. 21. The nonlinear sensitivity to c_7 is again obvious in the large jump as z passes through the neighborhood of 0.3. Two primary consequences of simulating with low wavelet resolutions are noted: (1) the actual c_7 bifurcation point can only be determined imprecisely relative to the full-order system, and (2) reducing the resolution of the simulations is somehow similar in effect to employing greater fifth-order stiffness in the full-order system, especially for high values of the random parameter, because the limit cycle amplitudes are lower than in the full model. This observation is based on the fact that the fifth-order stiffness terms in Eq. (34) are responsible for restraining the post-bifurcation oscillation amplitude. However, expansion resolution and fifth-order stiffness clearly should not be confused in this case because it was the third-order stiffness that was made random. The confusion arises because, as noted for the sinusoidal problem, reducing the resolution chops off the extreme values of the oscillations in the random dimension.

6. Concluding remarks and future work

Recent studies have shown that random variability in system parameters, loads, and BCs can induce significant changes in the stability of nonlinear aeroelastic systems. These factors motivate current research to

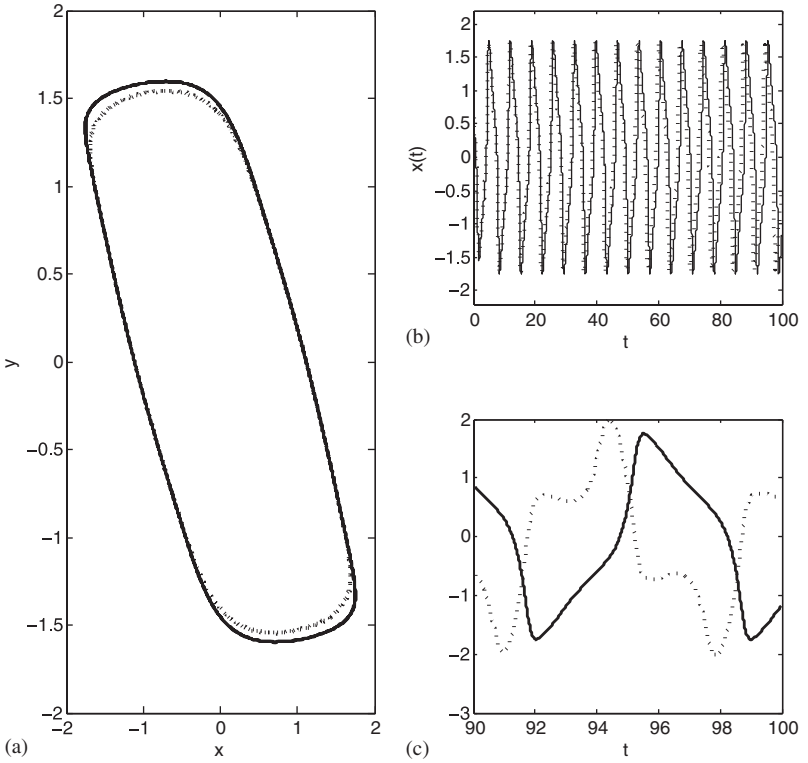

Fig. 20. Comparison of full model and $J = 5$ Wiener–Haar simulation for $z = 0.780$ or $c_7(z) = 0.890$: (a) phase plane plot of limit cycle; — full model, ⋯, Wiener–Haar; (b) $x(t)$; — full model, ⋯, Wiener–Haar; (c) close-up of (b) for full model, —, with overlay of expansion error, ⋯.

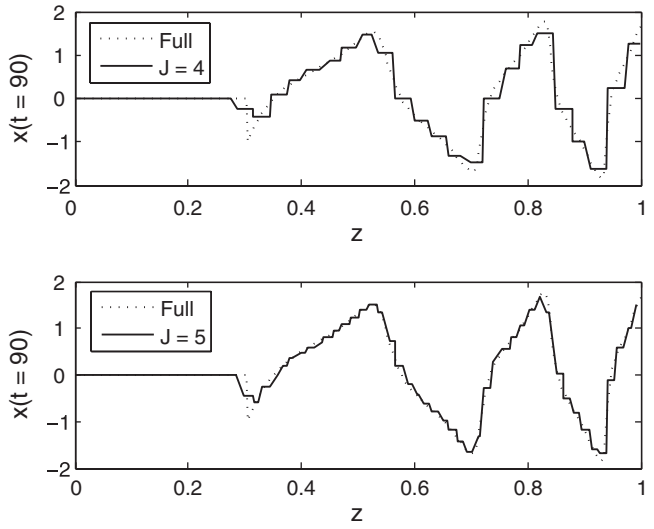

Fig. 21. Wiener–Haar simulation of $x(t)$ versus z at $t = 90.00$, with $c_7(z) = 0.5 + 0.5z$. The $J = 5$ expansion resolves better the sharp changes missed by the $J = 4$ expansion; (top) — $J = 4$, ⋯ original data; (bottom) — $J = 5$, ⋯ original data.

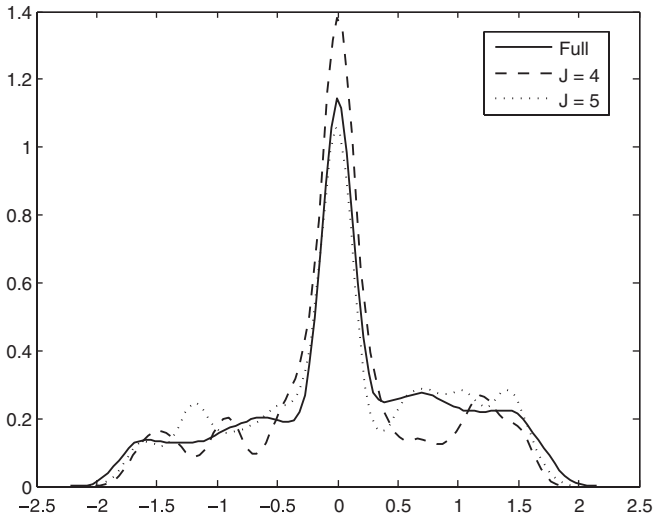

Fig. 22. Estimated density functions of $x(t)$ at $t = 90.00$ for original data and Wiener–Haar expansions. —, original data, - - - $J = 4$, ⋯, $J = 5$.

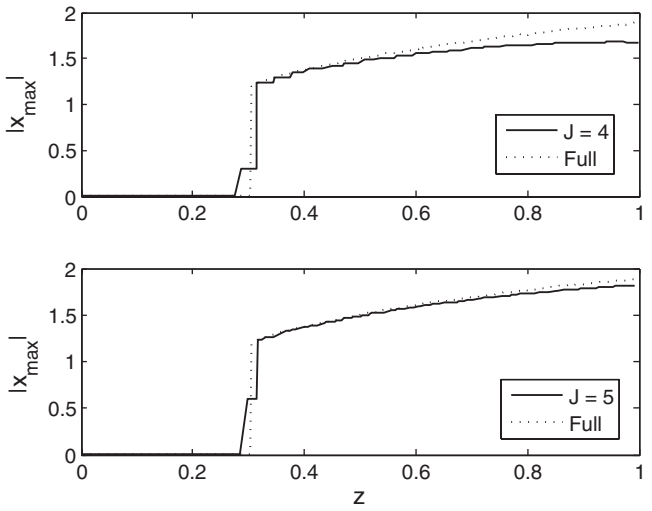

Fig. 23. Maximum value of $|x(t)|$ for $t \geqslant 80.00$; (top) — $J = 4$, ⋯, original data; (bottom) — $J = 5$, ⋯, original data.

substantially improve our ability to predict the range of behaviors a future aeroelastic system could exhibit. Stochastic expansions are expected to be an important tool in computational frameworks for high fidelity simulations of nonlinear aeroelastic systems, which commonly undergo bifurcations that lead to self-excited but stable oscillatory responses.

The key problem described above in using Wiener expansions to model a stochastic oscillatory process is the lack of long-term accuracy induced by the truncation of higher-order terms in the spectral basis for the random dimension. This problem is substantially resolved by employing a MRA in the random dimension. The Haar basis adapts naturally to the evolution of the frequency content in the random dimension as time passes, so that dominant features of the long-term response can be captured even by relatively low-order expansion.

Employing the WHa expansion for oscillatory stochastic systems has the additional advantage of providing a digital filter approach, known as Mallat's pyramid algorithm, to evaluating the expansion coefficients. It is found that the pyramid algorithm is substantially more efficient and accurate for evaluating WHa expansion

coefficients than MCS or numerical quadrature. However, practical use of the non-intrusive formulation described herein for simulating realistic systems will require more efficient time-accurate computations to enable quicker calculation of the WHa coefficients. Reduced-order methods are being considered for this role in future studies.

Acknowledgments

This work was supported in part by the Air Force Office of Scientific Research, Laboratory Task 03VA01COR (Program Manager: Dr. Fariba Fahroo). This support is greatly appreciated. The authors also wish to thank Professors Roger Ghanem (University of Southern California) and Omar Knio (The Johns Hopkins University) for introducing them to the Wiener–Haar expansion.

References

[1] AFOSR/AFRL Workshop on Nonlinear Aeroelasticity and Related Structural Dynamics, Shalimar, FL, 2003.
[2] F.M. Hoblit, *Gust Loads on Aircraft: Concepts and Applications*, AIAA Education Series, 1988.
[3] C.L. Pettit, P.S. Beran, Effects of parametric uncertainty on airfoil limit cycle oscillation, *Journal of Aircraft* 40 (5) (2003) 1004–1006.
[4] C.L. Pettit, Uncertainty in aeroelasticity analysis, design, and testing, in: E. Nikolaidis, D. Ghiocel (Eds.), *Engineering Design Reliability Handbook*, CRC Press, Boca Raton, FL, 2004.
[5] C.L. Pettit, D.E. Veley, Risk allocation issues for systems engineering of airframes, in: *Fourth International Symposium on Uncertainty Management and Analysis*, College Park, MD, 2003.
[6] C.L. Pettit, Uncertainty quantification in aeroelasticity: Recent results and research challenges, *Journal of Aircraft* 41 (5) (2004) 1217–1229.
[7] D.G. Liaw, H.T.Y. Yang, Reliability of uncertain laminated shells due to buckling and supersonic flutter, *AIAA Journal* 29 (10) (1991) 1698–1708.
[8] D.G. Liaw, H.T.Y. Yang, Reliability and nonlinear supersonic flutter of uncertain laminated plates, *AIAA Journal* 31 (12) (1993) 2304–2311.
[9] N.J. Lindsley, P.S. Beran, C.L. Pettit, Effects of uncertainty on nonlinear plate aeroelastic response, in: *43rd AIAA/ASME/ASCE/AHS/ASC Structures, Structural Dynamics, and Materials Conference*, Denver, CO, 2002 AIAA-2002-1271.
[10] N.J. Lindsley, P.S. Beran, C.L. Pettit, Effects of uncertainty on nonlinear plate response in supersonic flow, in: *Ninth AIAA/ISSMO Multidisciplinary Analysis and Optimization Conference*, Atlanta, GA, 2002 AIAA-2002-5600.
[11] N.J. Lindsley, P.S. Beran, C.L. Pettit, Effects of uncertainty on the aerothermoelastic flutter boundary of a nonlinear plate, in: *Eleventh AIAA/AAAF International Conference on Space Planes and Hypersonic Systems and Technologies*, Orleans, France, 2002 AIAA-2002-5136.
[12] R. Ghanem, P.D. Spanos, *Stochastic Finite Elements: A Spectral Approach*, revised ed., Dover Publications, New York, 2003.
[13] D. Xiu, G.E. Karniadakis, The wiener-askey polynomial chaos for stochastic differential equations, *SIAM Journal of Scientific Computing* 24 (2) (2002) 619–644.
[14] D.R. Millman, P.I. King, P.S. Beran, A stochastic approach for predicting bifurcation of a pitch and plunge airfoil, in: *21st AIAA Applied Aerodynamics Conference*, Orlando, FL, 2003 AIAA-2003-3515.
[15] C.S. Burrus, R.A. Gopinath, H. Guo, *Introduction to Wavelets and Wavelet Transforms*, Prentice-Hall, Upper Saddle River, NJ, 1998.
[16] O.P. Le Maître, O.M. Knio, H.N. Najm, R.G. Ghanem, Uncertainty propagation using Wiener–Haar expansions, *Journal of Computational Physics* 197 (2004) 28–57.
[17] D. Xiu, G.E. Karniadakis, Modeling uncertainty in flow simulations via generalized polynomial chaos, *Journal of Computational Physics* 187 (2003) 137–167.
[18] O.P. Le Maître, O.M. Knio, H.N. Najm, R.G. Ghanem, A stochastic projection method for fluid flow: I. basic formulation, *Journal of Computational Physics* 173 (2001) 481–511.
[19] R.W. Walters, Towards stochastic fluid mechanics via polynomial chaos, in: *41st AIAA Aerospace Sciences Meeting and Exhibit*, Reno, NV, 2003 AIAA-2003-0413.
[20] H. Stark, J.W. Woods, *Probability Random Processes and Estimation Theory for Engineers*, second ed., Prentice-Hall, Englewood Cliffs, NJ, 1994.
[21] M. Evans, T. Swartz, *Approximating Integrals via Monte Carlo and Deterministic Methods*, Oxford University Press, Oxford, 2000.
[22] R.E. Melchers, *Structural Reliability Analysis and Prediction*, Wiley, New York, 1999.
[23] C. Gasquet, P. Witomski, *Fourier Analysis and Applications: Filtering, Numerical Computation, Wavelets*, Springer, New York, 1999.
[24] G. Strang, T. Nguyen, *Wavelets and Filter Banks*, Wellesley-Cambridge Press, Wellesley, MA, 1996.
[25] R.T. Ogden, *Essential Wavelets for Statistical Applications and Data Analysis*, Birkhauser, Basel, 1997.
[26] R. Li, R. Ghanem, Adaptive polynomial chaos expansions applied to statistics of extremes in non-linear random vibration, *Probabilistic Engineering Mechanics* 13 (2) (1997) 125–136.
[27] S.H. Strogatz, *Nonlinear Dynamics and Chaos: with Applications to Physics, Biology, Chemistry, and Engineering*, Addison-Wesley, Reading, MA, 1994.